Intensity Stabilization of a Solid-State Laser for Interferometric Gravitational Wave Detectors

by

Jameson Graef Rollins

B.S., University of Michigan (1999)

Submitted to the Department of Physics
in partial fulfillment of the requirements for the degree of

Master of Science in Physics

at the

MASSACHUSETTS INSTITUTE OF TECHNOLOGY

February 2004

Author .....
Department of Physics
February 9, 2004

Certified by .....
Rainer Weiss
Professor of Physics
Thesis Supervisor

Accepted by .....
Thomas J. Greytak
Associate Department Head for Education

Intensity Stabilization of a Solid-State Laser for Interferometric Gravitational Wave Detectors

by

Jameson Graef Rollins

Submitted to the Department of Physics
on February 9, 2004, in partial fulfillment of the
requirements for the degree of
Master of Science in Physics

Abstract

A high-power, low noise photo-detector, in conjunction with a current shunt actuator has been used in an AC-coupled servo to stabilize the intensity of a 10 Watt continuous-wave Nd:YAG laser. A relative intensity noise of $1 \times 10^{-8}/\sqrt{\text{Hz}}$ at 10 Hz has been achieved.

Thesis Supervisor: Rainer Weiss
Title: Professor of Physics

Acknowledgments

First and foremost, I would like to thank my family: my mother, Stefanie, my father, Jim, and my brother, Stefan. Their love and support has always been unwavering and I love them all.

My faculty advisor, Rainer Weiss, has been one of the most inspiring persons that I have ever had the honor of knowing. The breadth of his knowledge, his passion for physics, and his outgoing straightforwardness put him squarely in class unto himself. Knowing him has been a humbling experience. I truly wish that I could have lived up to the standards that his legacy demands.

It has been a particular joy to work with my day-to-day advisor, Dave Ottaway. His good-nature and patience has guided my research over the last couple of years, yet he has managed to always treat me as an equal, and for that I am grateful.

David Shoemaker has been especially kind and supportive in my time at MIT. His willingness to listen to my problems and provide advice and support has helped me figure out where I am and where I'm going.

My fellow grad students, Ryan Lawrence, Rana Adhikari, and Shourov Chatterji, have been a constant source of humor, companionship and support. I will truly miss our late night discussions and smoke breaks. I expect them to all go far and I wish them the best of luck.

The other lab staff scientists, Mike Zucker, Nergis Mavalvala, Peter Fritschel, Gregg Harry, Rich Mittleman, and Pradeep Sarin, have been an incredible group of co-workers and have provided much needed and appreciated guidance.

I would also like to express my gratitude to the lab support staff for all of their invaluable practical help. The lab system administrator, Keith Bayer, has put up with all of my computer demands and has been a great comrade and friend. Myron MacInnis has kept me in check and has always been helpful, no mater how overworked he has been. Our secretary, Marie Woods, has always been completely unflappable and somehow manages to take care of any problem with ease.

My time with LIGO has been the most fulfilling of my life. I have met countless

incredible and fascinating people. I hope I get a chance to work with all of them again.

Finally, I would like to thank my girlfriend, Rebecca. She is one of the most kind and beautiful people I have ever met, and her comfort and support have helped me immeasurably. I love her dearly.

Contents

List of Figures

Introduction

The Laser Interferometer Gravitational-Wave Observatory (LIGO)[1] is one of the world's largest and most sensitive gravitational-wave detectors [3, 5]. The goal of LIGO is to detect gravitational waves of astrophysical and cosmological origin incident on the Earth. To date, direct observation of these waves has not occurred. Initial LIGO has a target displacement sensitivity of approximately 10^{-19} meters/$\sqrt{\text{Hz}}$ at 100 Hz over a baseline of 4 km.

Research and development has already begun on Advanced LIGO, a second-generation detector that will be housed in the same facilities. Advanced LIGO aims to improve upon the displacement sensitivity of Initial LIGO by over an order of magnitude [11, 9]. At the moment, Advanced LIGO is scheduled for installation in 2007.

LIGO uses long baseline Michelson-type interferometers to detect small differential motions of suspended test masses induced by gravitational waves. Interferometric gravitational-wave detectors of this type require highly stable laser light sources. The Advanced LIGO requirements for the frequency and intensity noise on the light entering the interferometer are quite stringent.

In this dissertation, I will describe work aimed at achieving the Advanced LIGO intensity noise requirement on an Initial LIGO pre-stabilized laser system using feedback control and a new high-power, low-noise photo-detector.

Chapter 1 will discuss the theory of laser intensity noise and how it affects the LIGO interferometer. Chapter 2 will be a description of the design and implementation of a low-noise, high-power photo-detector that was developed for these experi-

[1] http://ligo.caltech.edu/

ments. Chapter 3 will be a description of the LIGO pre-stabilized laser system that was used as a test bed for the intensity stabilization servo. Chapter 4 will discuss the intensity stabilization servo itself. Finally, Chapter 5 will discuss the results of the experiment. The expression for shot noise is derived in Appendix A; amplifier noise is described in Appendix B; Appendix C is a brief introduction to linear, time-invariant control theory; Appendix D and Appendix E are the photo-detector and servo board circuits, respectively.

This work, and the LIGO Laboratory, is supported by the National Science Foundation[2] under Cooperative Agreement No. PHY-0107417.

[2]http://www.nsf.org/

Chapter 1

Intensity Noise

1.1 Sources of intensity noise

In all precision optical measurements, stability of the light source is of utmost importance. Frequency, intensity, polarization and other instabilities of the light can cause noise in the measurement and reduce the sensitivity of the experiment.

Laser intensity noise is a random fluctuation in the power or amplitude of the laser beam. It can be caused by many things, both internal and external to the laser light source itself. In fact, fluctuations in any of the parameters of a laser beam can in one way or another affect the intensity of the beam as measured in an optical experiment [12, 17, 7].

Intensity noise generated inside of the laser usually comes from two places. The laser intensity is controlled by current to the laser pump diodes. If that current fluctuates, so will the laser intensity. Optical path fluctuations inside of the laser's resonant optical cavity can also cause output intensity fluctuations due to deviations from exact resonance of the cavity.

External to the laser source itself, many environmental factors can affect the beam and lead to intensity noise. A common source of intensity noise is particles falling through the path of the beam. When a particle falls through the beam path, it causes photons to be randomly scattered out of the beam, thereby reducing the beam intensity.

Changing indices of refraction of the medium through which the beam is passing can also generate noise. If the beam is passing through air or other gases, air currents cause random pressure differentials that lead to fluctuations in the index of refraction. This can cause the beam path to fluctuate and produce beam jitter.

Beam jitter can be a major problem in intensity measurements [10]. Beam jitter will cause fluctuations in coupling efficiency at the input to optical cavity resonators and in the transmission of defining apertures. Both phenomena result in intensity fluctuations measured at the detector.

Movement of the beam over the surface of the detector is another source of measured intensity noise. The mechanism in this case are the spatial variations of the detector sensitivity which cause time varying photo-currents as the beam jitters over the detector surface. Due to these effects, it is often necessary to stabilize the beam geometry in precision optical measurements to attain maximum sensitivity.

Intensity noise can also be the by-product of fluctuations of other parameters of the beam, such as frequency and polarization. For example, the reflectivity and transmissivity of mirrors and beam splitters are a function of the polarization of the incident beam. Random polarization fluctuations can cause variations in the amount of the beam that is reflected or transmitted, which can cause intensity noise. Interference is affected by the light frequency and phase. Any process that depends on interference, such as coupling into optical cavities and scattered light on detectors, can cause intensity noise if the frequency or phase is fluctuating.

1.2 Intensity noise control

The first thing needed to control intensity noise is to eliminate as many of the external sources of noise as possible. For instance, intensity noise caused by particles moving through the path of the beam or air currents can be significantly reduced by enclosing the beam path in a vacuum or other clean enclosure.

Once external noise sources have been significantly reduced, intensity noise is further suppressed with the use of negative feedback control. The basic idea is that

the intensity noise is measured by comparing the photo-detector output against a fixed reference. The difference between these signals (the error signal) is then filtered, amplified, inverted, and then fed into an actuator up-stream of the detector, often within the laser itself.

Feed-forward can also be used to control intensity noise. Feed-forward is a technique similar to feedback, except that the point of actuation is down-stream of the detector. A detector measures the noise and produces an error signal. The negative of this error signal is then fed into an intensity actuator down-stream from the detector. Feed-forward requires precise foreknowledge of the transfer function from the measured excitation to the change in intensity of the actuator.

1.3 Intensity noise in LIGO

Laser intensity fluctuations limit the sensitivity of interferometers through several mechanisms. The first is through directly masking the signal at the detector, generally known as gain modulation. The second is the through the effect of radiation pressure on the test masses.

Radiation pressure on the sensing mirrors, which in the case of gravitational wave detectors are suspended test masses in the range from 1 to 40 kg. The impact of photons on the suspended test masses transfers a small amount of momentum to the test masses that is proportional to the light power. Fluctuations in the power levels inside the interferometer cause a fluctuating force to be applied to the test masses, thereby causing displacement noise.

Fluctuating power levels at the detector can also cause an effect known as *gain modulation*. Gain modulation is a term used to describe various effects whereby intensity noise masks the signal at the detector. For instance, when the experiment output is meant to have a very small or vanishing signal (also known as a *null signal*), yet there is a large amount of junk light that is of no interest to the experiment, amplitude fluctuations on this junk light will disturb the measurement.

Of particular importance to LIGO is a type of gain modulation involving non-

linear conversion of out-of-band signals into the band of interest. If the detector signal is meant to be null but there is a signal out of the band of interest, called out-of-band noise, then intensity noise on the light will produce signals at the product of the intensity noise and the out-of-band noise. This will cause frequency components at the sum and difference of the intensity spectrum and the out-of-band noise and harmonic multiples. This process is also referred to as *bilinear conversion*, and may turn out to be a limit on the LIGO interferometer performance.

1.4 Advanced LIGO

Next generation gravitational wave detectors will be more sensitive to intensity noise since they require very high circulating power. Photon counting errors, also known as shot noise (Appendix A) will be the dominant noise source at frequencies above a few hundred hertz. The contribution of this noise source to the strain sensitivity of the instrument is proportional to the square root of the incident laser power. Since the signal increases linearly with power, increasing the circulating power will therefore increase the signal-to-noise ration (SNR) by a factor of the square root of the power. However, increasing the circulating power will in turn increase sensitivity of the interferometer to technical intensity noise [11, 9].

The required relative intensity noise performance for Advanced LIGO is shown in Fig. 1-1. The *relative intensity noise* is defined as the fluctuation in the intensity per unit bandwidth of frequency, divided by the mean intensity noise over the measurement interval, $I(f)/\langle I\rangle$, and has units of $1/\sqrt{\text{Hz}}$. The most demanding part of the Advanced LIGO requirement is $2\times10^{-9}/\sqrt{\text{Hz}}$ at 10 Hz.

Current plans for Advanced LIGO call for the use of a 180 Watt laser system [24] which may be of a different design than the system used in Initial LIGO. This higher power system may be accompanied by higher relative intensity noise levels, which may require more servo gain to reach the same relative intensity noise level. Other than issues of servo gain, the main hurdles to achieving excellent intensity noise performance in a stabilized laser are sensor noise, non-linearities in servo electronics,

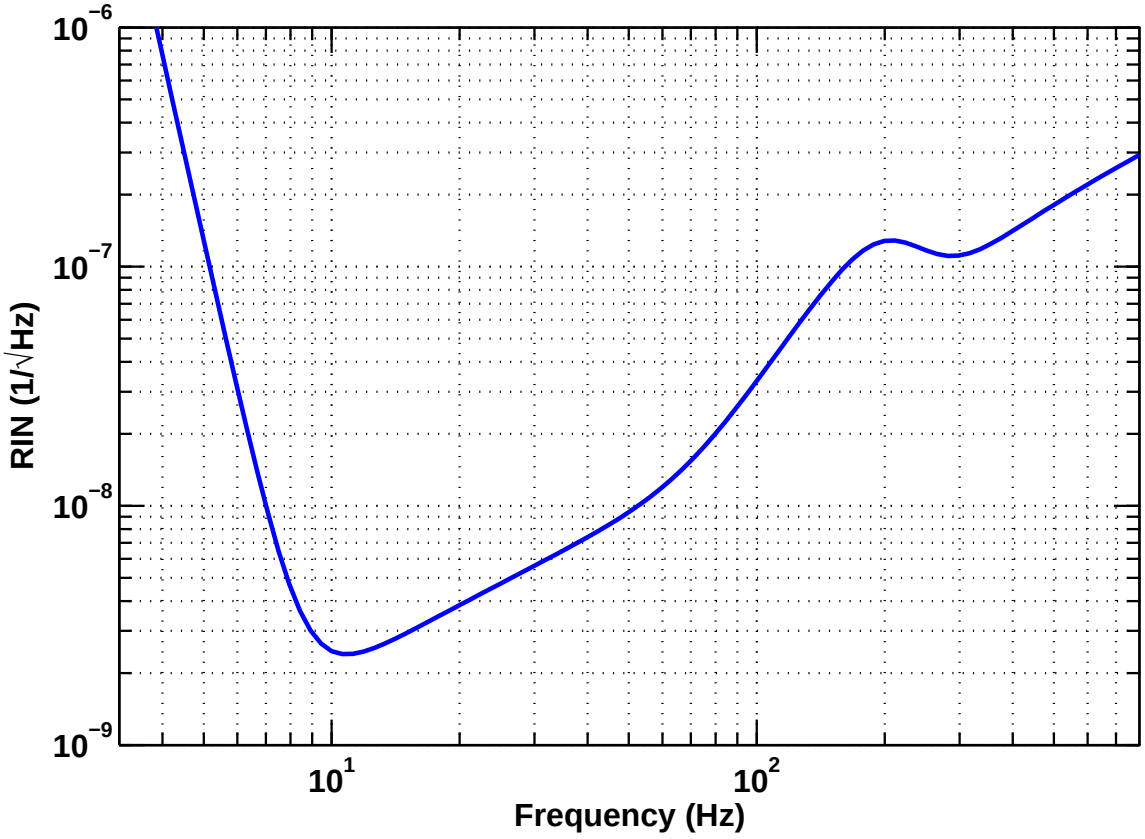

Figure 1-1: Advanced LIGO relative intensity noise requirement [9].

and beam geometry fluctuations. These other limitations are common to any of the configurations that would be used in Advanced LIGO, and therefore the system used to control the intensity noise of an Initial LIGO laser, such as the one used for the experiments in this thesis (see Chapter 3), will be applicable to Advanced LIGO as well.

Chapter 2

The Low-noise, High-power Photo-detector

2.1 Detector requirements

Assuming that the only limit to achieving a relative intensity noise level of $2 \times 10^{-9}/\sqrt{\text{Hz}}$ is the detection of laser shot noise, to achieve an overall intensity noise level of $2\times10^{-9}/\sqrt{\text{Hz}}$, two photo-detectors in parallel would have to each see a shot noise level of at least a factor of $\sqrt{2}$ less than that, or about $1\times10^{-9}/\sqrt{\text{Hz}}$ (see Section 4.1 for a discussion on the necessity of two detectors). We therefore set as a requirement of the photo-detector the detection of a relative intensity noise of $e_{\text{rin}} = 1\times10^{-9}/\sqrt{\text{Hz}}$.

The expression for laser shot noise, derived in Appendix A, is given by

$$e_{\text{shot}}(f) = \frac{P(f)}{\langle P \rangle} = \sqrt{\frac{hc}{\lambda \langle P \rangle}}, \tag{2.1}$$

where $P(f)$ is the power fluctuation, $\langle P \rangle$ is the mean of the power, h is Planck's constant, c is the speed of light, and λ is the frequency of the light. Equation 2.1 is a relative intensity noise amplitude spectral density and has units of $1/\sqrt{\text{Hz}}$. By setting $e_{\text{rin}} = e_{\text{shot}}$ and substituting in from Equation 2.1, we can easily determine the two numbers relevant to the design of a suitable shot noise limited photo-detector: $P(f)$ and $\langle P \rangle$.

These experiments use a solid-state Nd:YAG laser with a single-frequency output wavelength of $\lambda = 1064$ nm (see Chapter 3). Substituting this in for λ along with the well known values of h and c, we get a value of the required light power at the detector of

$$\langle P \rangle = \frac{hc}{\lambda e_{\text{rin}}^2} \approx 0.373 \text{ Watts.} \tag{2.2}$$

A value for the power fluctuations that we must be able to detect follows:

$$P(f) = e_{\text{rin}} \times \langle P \rangle = \frac{10^{-9}}{\sqrt{\text{Hz}}} \times \langle P \rangle = 373 \times 10^{-12} \, \frac{\text{Watts}}{\sqrt{\text{Hz}}}. \tag{2.3}$$

From the calculations above, we see that to detect shot noise at the level of $10^{-9}/\sqrt{\text{Hz}}$, we must be able to detect a change in power of roughly 400 pW$/\sqrt{\text{Hz}}$ on top of a DC power level of 400 mW.

2.2 The photo-diode

The photo-detector uses as its light sensitive element a *photo-diode*. Photo-diodes are one of many devices used to turn photons into an electrical current. They are used here because of their simplicity, low power requirements, and near quantum-limited sensitivity. I will not go too deep into the theory of operation here since there are many sources that cover that in detail [18, 16]. The basic principle is that the photo-diode is a diode under a reverse bias voltage. When a photon strikes the diode, it is absorbed by an electron, bumping it out of the depletion layer and into the conduction band where it is swept away by the reverse bias and turned into an output photo-current.

The efficiency of this conversion from photon to photo-electron is given by a characteristic of the photo-diode known as the *quantum efficiency*. The quantum efficiency is a measure of how many photo-electrons are produced, on average, by each photon hitting the diode. It is made up of the transition probability of exciting an electron into the conduction band, the fraction that are collected into the current measured at the electrodes, and the absorption of light by the material itself that

does not produce charge carriers (otherwise known as *lattice absorption*). In the case of photo-diodes, the quantum efficiency is a number less than one and a perfect quantum efficiency would mean that each photon produces a single photo-electron. Most InGaAs photo-diodes, like the kind used here, have quantum efficiencies above 90%. Silicon photo-diodes, on the other hand, tend to have quantum efficiencies much lower.

The conversion from light power to current is given by the following formula:

$$\langle I \rangle = \gamma \frac{e}{h\nu} \langle P \rangle = \gamma \cdot 1.164 \cdot \langle P \rangle, \tag{2.4}$$

where e is the charge of the electron and γ is the quantum efficiency.

To determine the requirements on the photo-diode in our photo-detector, simply combine Equations 2.2 and 2.3 with Equation 2.4:

$$\langle I \rangle = 320 \text{ mAmps} \tag{2.5}$$

$$I(f) = 320 \ \frac{\text{pAmps}}{\sqrt{\text{Hz}}}. \tag{2.6}$$

These requirements on the photo-diode are particularly extreme, and will therefore require various improvements to traditional photo-detector designs.

The actual photo-diodes that were chosen for the detector are Hamamatsu G5832-02 2 mm InGaAs photo-diodes. These were chosen because of their demonstrated ability to handle fairly large power levels, as well as for their high surface uniformity and quantum efficiency. They are measured to have a quantum efficiency of 93%.

2.3 Detector layout

Photo-diodes are usually read out by the use of a *trans-impedance amplifier*. In this configuration, the anode of the diode is attached to the inverting input of a operational amplifier which is held at a virtual ground by grounding the non-inverting input [13, page 184]. In this case, the amplifier provides a sink for the photo-current via the feedback to the inverting input.

The trans-impedance configuration is convenient since it provides a direct translation of the photo-current into a voltage output of the op-amp. However, it also has some limitations that make it unsuitable for the detection of extremely low shot noise levels at high powers. As was shown in Equation 2.6, detecting a shot noise level of 10^{-9} requires very low-noise op-amps. However, one must simultaneously detect more than 300 mA of DC photo-current. Together, this makes the use of trans-impedance amplification difficult. Low noise op-amps generally can not sink such high current loads. This required the design of an alternative detection scheme.

It was decided that a more effective approach would be to use an older technique that employs a separate load resistor. Instead of having the read out pre-amplifier sink all of the photo-current itself, the bias and current supply are handled by a voltage regulator. The photo-current from the diode is then sunk directly across a resistor to ground. This resistor converts the photo-current into a voltage. The AC and DC components of this voltage can then be read out individually by high input impedance, low-noise operational amplifiers of significantly different gain. In this case, the detector is able to handle both low noise and high current by dividing the task.

A simplified schematic of the final photo-diode read-out circuit can be seen in Figure 2-1 (See Appendix D for a full circuit schematic). On the left side of the schematic is the bias feedback control circuitry described in the next section, while the right side of the schematic is the read-out amplifiers.

2.4 Bias voltage and current supply

The detector employs a bias feedback control circuit to maintain a constant bias voltage across the photo-diode regardless of the photo-current. This serves two purposes. The first is to reduce the amount of power dissipated over various light powers. The power dissipation across the diode is of particular concern since such high light powers are used. Heating caused by power dissipation can damage the photo-diode.

The second concern is that if a fixed voltage is used to supply the bias, fluctua-

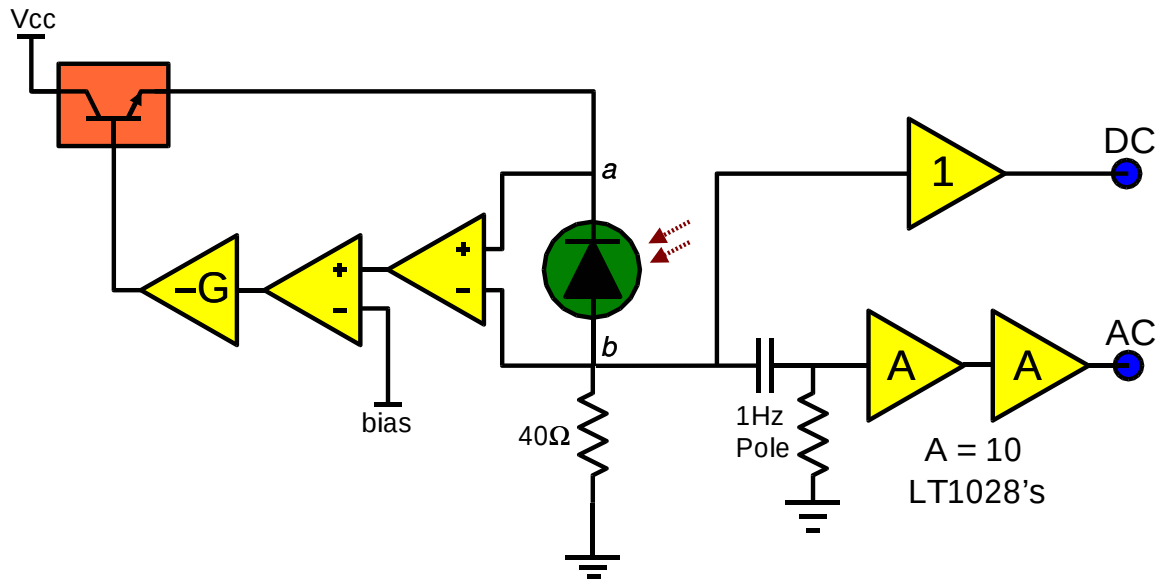

Figure 2-1: Schematic of the photo-detector circuit.

tions in the light level, and therefore the photo-current, would result in a fluctuating voltage across the photo-diode. This would in turn cause changes in the photo-diode capacitance and affect the high frequency response of the photo-diode.

On the left side of Figure 2-1 one can see the photo-diode current supply and bias voltage circuitry. Current is supplied by a National Semiconductor LM317 voltage regulator. The bias voltage is controlled by a feedback circuit. First, the voltage across the photo-diode is read off with a differential amplifier. A voltage reference, v_{bias}, which can be externally controlled, is added to this, and the signal is then amplified and fed into the base of the voltage regulator. The voltage regulator maintains a set voltage, v_e, between its base and its emitter. The voltage at the top of the photo-diode is

$$v_a = -G(v_a - v_b - v_{bias}) + v_e. \tag{2.7}$$

After a little bit of algebra (see Appendix C), we can see that

$$v_a = \frac{G}{1+G}(v_b + v_{\text{bias}}) + \frac{1}{1+G}v_e. \tag{2.8}$$

With $G \gg 1$, this equation can be simplified to

$$v_a = v_b + v_{\text{bias}} \tag{2.9}$$

$$v_{\text{pd}} = v_a - v_b = v_{\text{bias}}. \tag{2.10}$$

The bias voltage across the photo-diode, v_{pd}, can then be controlled by setting v_{bias}. This is useful in determining optimal bias voltage for the diode.

2.5 Read-out pre-amplifiers

The photo-current leaving the photo-diode is first sunk across a 40 Ω resistor known as the *load resistor* which turns the photo-current into a voltage that can then be filtered and amplified. The load resistor value of 40 Ω is used to achieve the highest possible signal-to-noise ratio.

The signal is nothing more than $V = IR$, where I is the photo-current, and $R = 40\ \Omega$. For the photo-currents in Equation 2.6, the signal voltages at the output of the photo-diode are:

$$\langle V \rangle \approx 12 \text{ Volts} \tag{2.11}$$

$$V(f) \approx 12\ \frac{\text{nVolts}}{\sqrt{\text{Hz}}}. \tag{2.12}$$

The $\langle V \rangle$ of this equation is in fact the error signal for the intensity stabilization servo. It is this signal that is AC coupled, amplified, and sent out to the servo electronics.

The AC coupling is achieved by a simple high-pass filter with a corner frequency at 1 Hz. The frequency of this cut-off should be as far below 10 Hz as possible so as not to degrade the signal-to-noise ratio at 10 Hz. However, cut-off frequencies much below 1 Hz would have required excessively large capacitors that would have been difficult to integrate into the photo-detector design.

After the AC coupling filter there are two identical pre-amplifier stages in series to amplify the signal to the output. Each stage is noninverting with a gain of 10, for

a total amplification within the detector of 111.

2.6 Detector noise

A servo is most susceptible to noise at the front end where the error signal is generated, i.e., the first amplification stage of the detector. In order to achieve the best possible performance, we must achieve the best possible signal-to-noise ratio at this point. For a SNR of at least 10, we require that the photo-detector *dark noise*, or noise level with no light incident on the diode, be no more than a few nVolts/$\sqrt{\text{Hz}}$ at the frequency where we expect to be most sensitive, which in this case is 10 Hz. The two things that contribute to noise at this point are the thermal electronic or *Johnson* noise of the resistive part of the load impedance, and the input-referred voltage noise of the first amplification stage (see Appendix B).

Johnson noise is a function of resistance and temperature and is given by the formula,

$$e_{\text{Johnson}} = \sqrt{4kTR} \tag{2.13}$$

where k is Boltzmann's constant, T is the absolute temperature in Kelvin, and R is the load resistance. Since Johnson noise goes as the square root of the resistance, increasing the sink resistance increases the signal-to-noise ratio since the signal increases as R. The resistor used for the load, as already mentioned, is set at 40 Ω since that produces the highest signal allowed by the detector amplifiers and power supply.

The amplifier input voltage noise is controlled by proper selection of op-amps and careful consideration of the amplifier gain and the components used to control it (see Appendix B). We chose to use ultra low noise Linear Technology LT1028 Operational Amplifiers which have, at 10 Hz, an input referred voltage noise of 1 nVolts/$\sqrt{\text{Hz}}$ and current noise of 12 pAmps/$\sqrt{\text{Hz}}$. Using this with the results of Appendix B we were able to create pre-amplifiers for the detector with an overall input referred voltage noise of 3 nVolts/$\sqrt{\text{Hz}}$.

Figure 2-2 is a plot of the dark noise output of the two detectors use for the

experiments. The plot also includes a line indicating the level that was calculated from a model of the photo-detector.

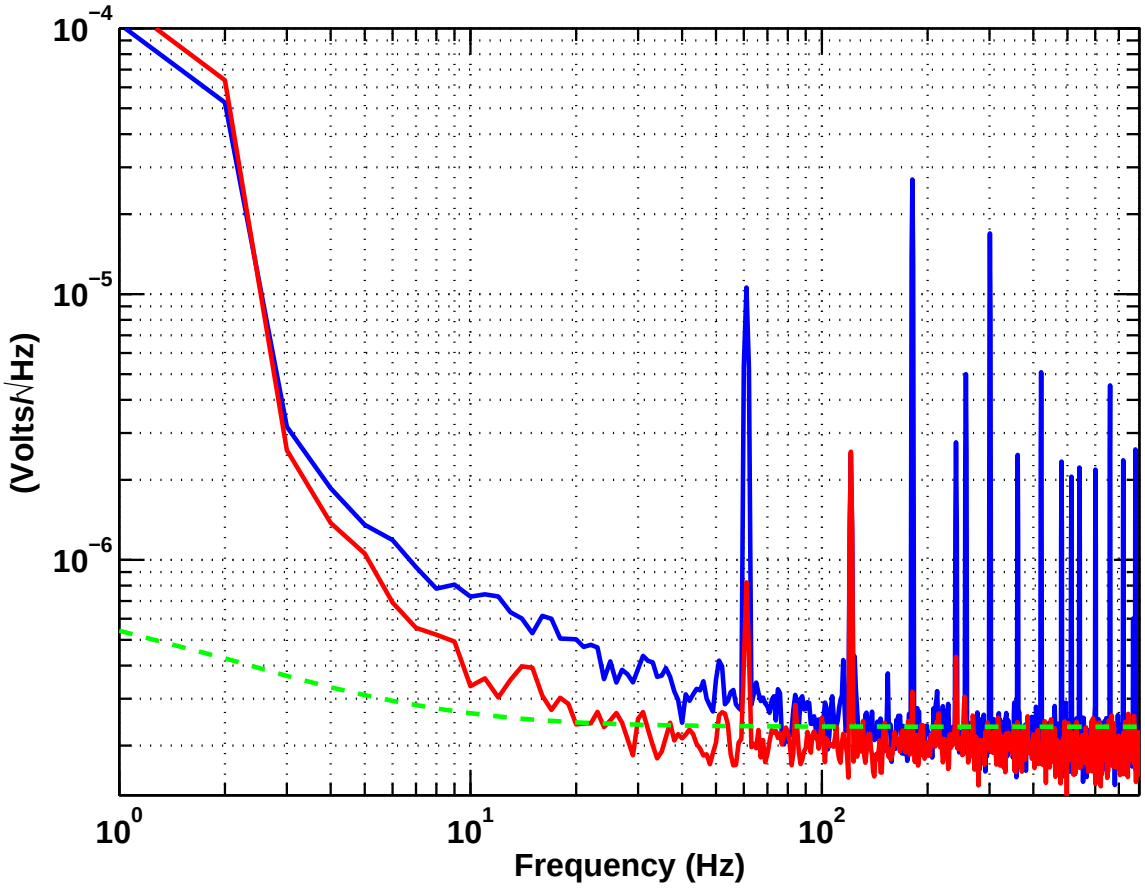

Figure 2-2: Measurements of the dark noise of both detectors used for the experiments (blue and red). The green line (dashed) is the dark noise level predicted by the model of the detector.

Careful consideration was also given to the effects of noise outside the servo bandwidth. It is well known that high frequency noise can encounter slew rate limits in any of the amplification stages, causing broad-band noise that would infect the sensitivity region of the frequency spectrum. While this is true throughout the servo chain, it is especially important at the front end. Low-pass filtering was used at both pre-amplification stages by including poles at 100 kHz.

Chapter 3

The Pre-Stabilized Laser

The LIGO requirements on frequency and intensity stability of the light entering the interferometer are very stringent. In order to achieve these stringent requirements, LIGO uses what is known as a Pre-Stabilized Laser (PSL) system [1].

The PSL consists of the laser light source, followed by multiple stages of frequency and intensity stabilization. Each of these stages is described below.

The laser that was used to test and develop this intensity stabilization system is a Pre-Stabilized Laser (PSL) system that is nearly identical to the PSL system that is used in initial LIGO.

3.1 The master-oscillator, power-amplifier laser

The light source for the PSL is a 10 W master-oscillator, power-amplifier (MOPA) laser made by Lightwave Lasers [14]. These types of lasers work by sending the light from a lower power, single frequency, low noise laser through multiple stages of amplification in order to achieve much higher light powers [21].

In our case, the master oscillator is a 700 mW single-frequency, single-mode non-planar ring oscillator (NPRO) laser that emits light at the 1064 nm line of the crystal Nd:YAG. The light from the master oscillator then passes through a series of diode-pumped power amplification stages also made of Nd:YAG. These amplifiers are able to bring the total light output of the MOPA up to 10 watts.

3.1.1 Laser current actuators

The MOPA has two main diode current adjustment actuators that are useful to the intensity stabilization servo. Both actuators modulate the current to the main power amplifier diodes of the laser.

The AC current adjust actuator (ACA) sums in directly to the power amplifier pump diode current supply at the MOPA control box. It has a response of about ±2.5 Amps/Volt up to 20 kHz, which is about 10% of the total drive current. After 20 kHz, the response falls off very steeply at a rate of about 80 dB/decade.

The current shunt (CS) [2] is a circuit in parallel with the power amplifier pump diodes and able to modulate the current at ±250 mAmps/Volt, or 1% of the full range. The response is flat up to 3 kHz, where there is only a single pole, making this actuator useful to much higher frequencies.

The frequency response measurements were made of both actuators and can be seen in Figure 3-1. For each measurement, each actuator was driven with a swept sine and one of the photo-detectors described in Chapter 2 was used to record the laser power response. The response in the plots is then the ratio of the voltage output of the photo-detectors, divided by the input drive voltage.

3.2 The pre-modecleaner

After the laser beam leaves the MOPA, it passes through a monolithic triangular cavity known as the pre-modecleaner (PMC) [22]. This cavity is locked to the laser frequency [1, 6] by actuating on a piezoelectric transducer attached to the rear mirror of the cavity.

The PMC acts as a high precision spatial mode filter by allowing only light that is mode matched to one of its resonant spatial transverse electro-magnetic (TEM) modes to pass through. The mode that is required in this context is the fundamental, TEM_{00} mode of the beam. This *modecleaning* reduces laser beam geometry fluctuations by a factor of several hundred. This is of particular importance to this experiment since laser beam jitter coupled with spatial imperfections are a major source of noise when

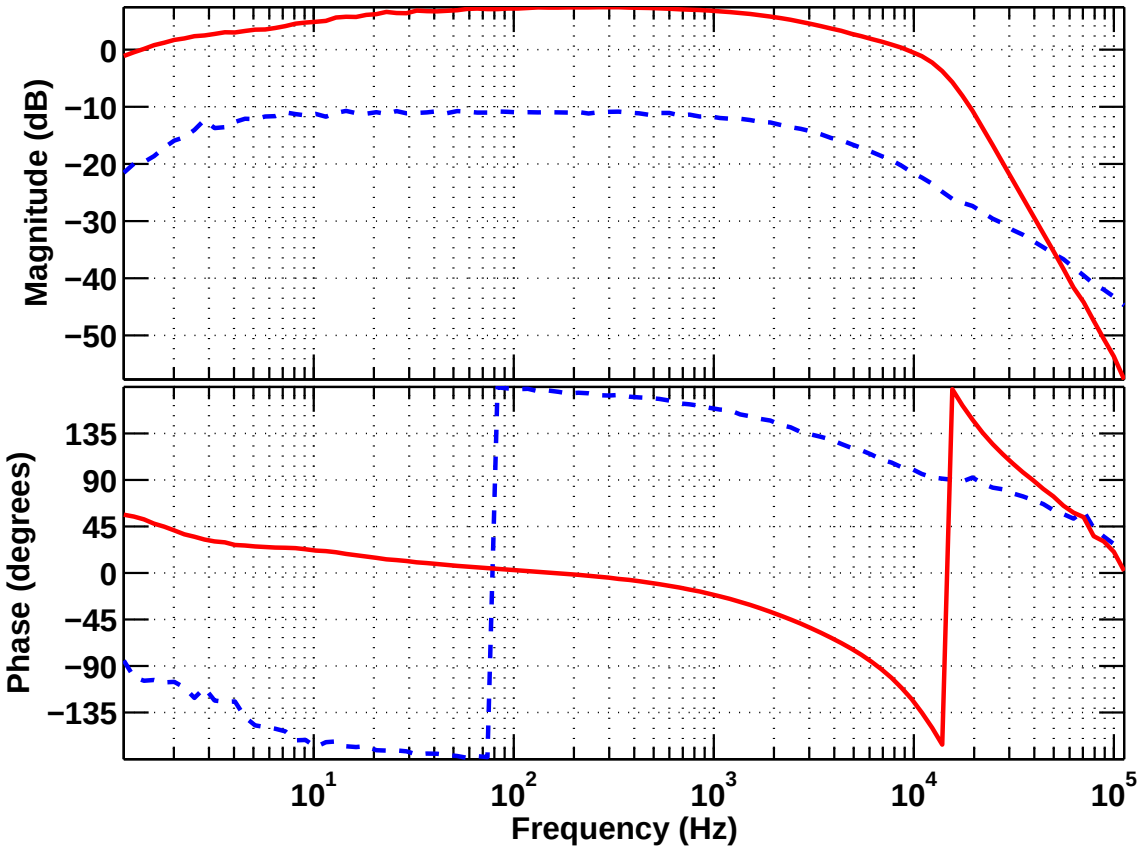

Figure 3-1: Frequency response of the AC current adjust and current shunt actuators. Swept sines were injected into the actuators and the response was measured by AC coupled photo-diodes after the PMC. The red curve (solid) is the AC current adjust response, while the blue curve (dashed) is the response of the current shunt.

dealing with low frequency intensity stabilization [10].

The PMC also acts as a low-pass filter with a frequency cut-off at the cavity resonance half-width, half-max of 1.5 MHz. This ensures that the light is near shot-noise limited for the RF sidebands used for locking the main interferometer. Being well outside of the intended bandwidth of the intensity stabilization servo control system (30 kHz) (see Section 4.2), this has no impact on the design of the intensity control servo.

3.3 The frequency stabilization servo

The frequency stabilization is achieved by picking off a small portion of the beam after the PMC and using it to lock the laser frequency to a very stable reference cavity [1, 6].

Because of the high bandwidth ($\sim$ 1 MHz) and dynamic range (several GHz) requirements, three different actuators with different dynamic ranges are used to feedback to the laser frequency in different frequency bands. There is a slow path that adjusts the temperature of the NPRO in the master-oscillator, a fast path that controls a piezoelectric transducer on the NPRO laser crystal, and a phase-adjust path that actuates on a Pockel's cell and adjusts the light phase at very high frequencies.

Chapter 4

The Intensity Stabilization Servo

Like almost every other LIGO subsystem, intensity noise in LIGO is suppressed by the use of feedback control. This chapter will discuss the implementation of an intensity stabilization servo on an initial LIGO PSL (see Chapter 3). I have deferred the basic introduction to feedback control for Appendix C, while this chapter will focus entirely on how to put the theory to practical use in the design of the servo.

The laser output intensity is a function of the current in the laser amplifier pump diodes. It is therefore the current to the diodes that needs to be modulated to control the laser intensity noise. In this servo, the laser intensity is measured with the photo-detector described in Chapter 2. The photo-detector output is the error signal that is then filtered and amplified by the servo electronics. Finally, the output of the servo electronics is fed back to the current actuators on the laser described in Section 3.1.1. In this way the laser intensity noise can be reduced by at most a factor of one over the total open-loop gain of the servo. We refer to this control system as the Intensity Stabilization Servo (ISS).

4.1 Servo layout

The physical layout of the servo is extremely important to its success. As mentioned in Section 1.1, the importance of beam stability in high-precision intensity measurements behooves us to find a suitable pick-off point to detect the intensity noise where beam

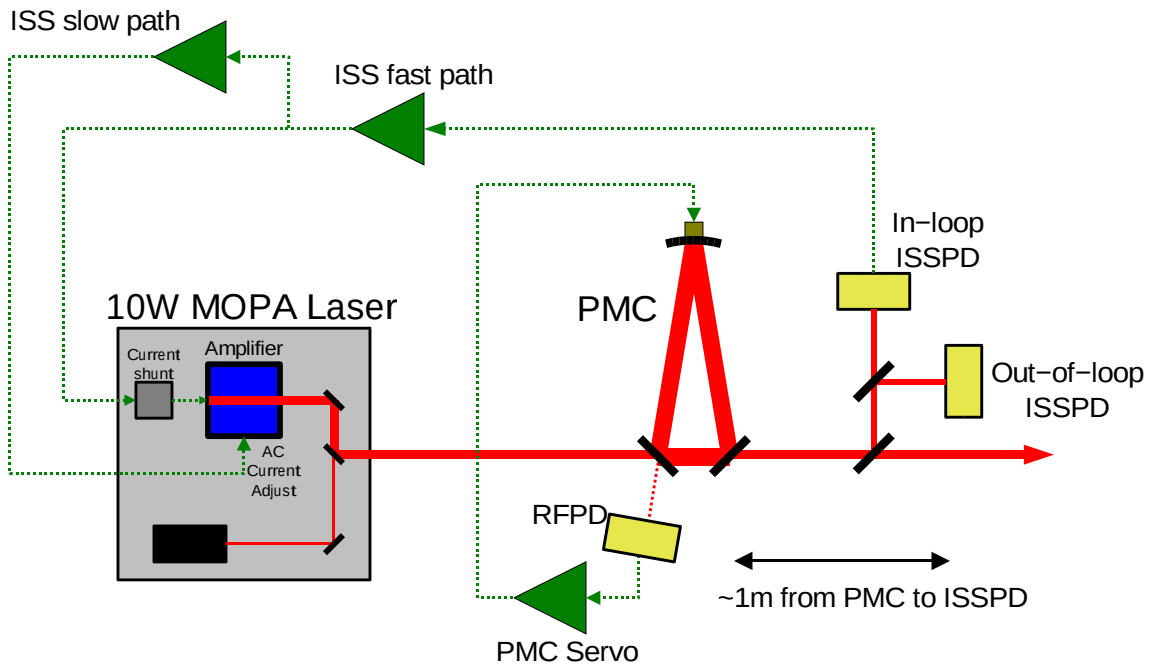

Figure 4-1: Schematic diagram of intensity stabilization servo. The *fast path* uses the fast current shunt actuator, whereas the *slow path* utilizes the low-bandwidth, high dynamic range AC current adjust actuator.

jitter is at a minimum. The most stable point in the PSL is directly down stream of the PMC. This allows us to take advantage of the beam-stabilizing effects of the PMC.

At the detection point, the beam is split and two photo-detectors are used to detect the beam. The first, known as the *in-loop* photo-detector, is what provides the error signal for the servo. The second, known as the *out-of-loop* photo-detector, is used for making measurements of the residual intensity noise. The in-loop detector can not be used for making measurements of the actual intensity noise since it is an erroneously low measure of the actual residual intensity noise (see Section C.6 for a discussion of why this is the case).

A schematic diagram of the full experimental layout is shown in Figure 4-1. The photo-detector detects the light about 1 meter beyond the output of the PMC to provide room for various optical elements.

Although the PMC provides a high degree of polarization discrimination for the

beam, a 1/2 wave plate and polarizing beam splitter cube are used for further polarization purification of the beam, as well as to control the total power reaching the photo-detectors. A lens was used to focus the beam on to the photo-detectors. Finally, a non-polarizing beam splitter is used to split the beam between the in-loop and out-of-loop photo-detectors.

4.2 Servo design

The goal of this intensity stabilization servo was to achieve a relative intensity noise of $2\times10^{-9}/\sqrt{\text{Hz}}$ at 10 Hz. The requirements this put on the design of the servo are largely determined by the free running intensity noise of the laser. Figure 5-1 includes a plot of the free running laser intensity noise. The free running noise level at 10 Hz is about $1\times10^{-5}/\sqrt{\text{Hz}}$. This means that a suppression of at least a factor of 10,000, or 80 dB, is needed at 10 Hz.

The frequency response measurements of the actuators and photo-diode made in Figure 3-1 are actually measurements of the entire system to be controlled. From an accurate knowledge of the frequency response of this system, one can construct the required servo response to produce the desired open loop gain curve.

The characteristic of the plant that made the design of the servo a bit tricky is that it is AC coupled. Although this makes the design of the servo slightly more complicated, by adding a lower unity gain point, it bypasses the need for a highly stable external DC reference; It also overcomes other issues in the design of the photo-detector discussed in Chapter 2, such as difficulty driving large load currents with low noise op-amps.

Another complication was the discovery that the current shunt alone does not have enough dynamic range below 1 Hz to control the free-running laser intensity noise. To circumvent this problem, the control signal to the current shunt is picked-off so that a separate signal could be fed back to the high dynamic range AC current adjust actuator. The path that feeds back to the AC current adjust is known as the *slow path*, whereas the path to the current shunt is know as the *fast path*. How to deal

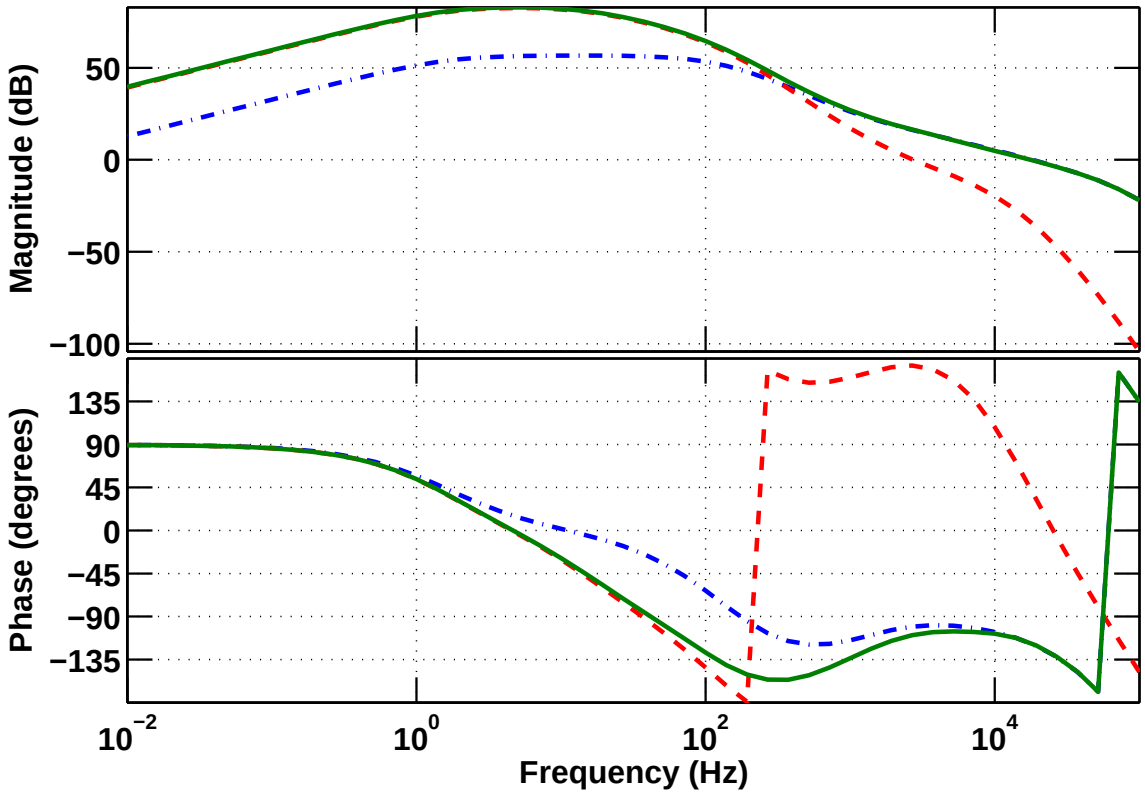

Figure 4-2: Plot of the required full servo open-loop frequency response (green curve, solid) from a model of the ISS. The blue curve (dash-dot) shows the requirement for the fast path alone, while the red curve (dashed) is the requirement for the slow path.

with these two paths and their interaction will be discussed in the next section.

Putting all of these considerations together, a required total open-loop frequency response of the full system can be constructed. The limits of the current shunt determine the shape of the gain at high frequencies. Since the response of the current shunt begins to fall off more quickly after 10 kHz, we then shoot for an upper unity gain point of 10 kHz. The combination of the AC coupling of the photo-detector at 1 Hz and the requirement of 80 dB of gain at 10 Hz determines the behavior at the low frequency end.

Figure 4-2 show a frequency response Bode plot of the full servo open-loop gain requirement from a model of the full servo system. The plot also includes the requirements for both the fast and slow paths individually, as will be discussed in the next section.

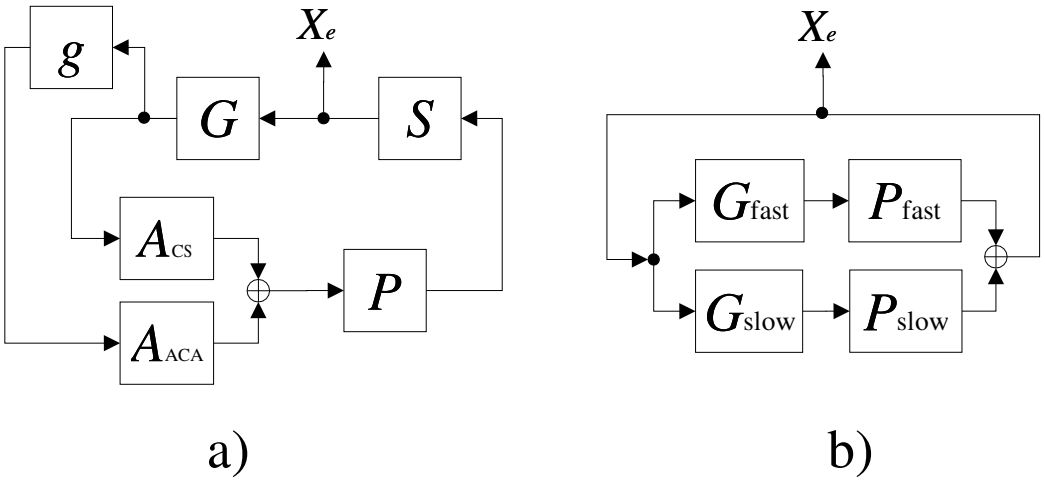

Figure 4-3: a) Block diagram of the full servo. b) Simplified block diagram.

4.3 Servo model

Figure 4-3a shows a simplified block diagram of the entire intensity stabilization servo (see Appendix C.1) where each block represents the transfer function of one of the servo components. In this case, P is the laser, S is the photo-detector, G is the common servo amplifier, g is the auxiliary filter for the slow path, and $A_{\rm CS}$ and $A_{\rm ACA}$ are the current shunt and AC current adjust transfer functions respectively.

Figure 4-3b shows a further simplification of the block diagram in 4-3a to a form that is more useful for this design since it more closely resembles the measurements of the system from Figure 3-1. Here we make the definitions:

$$\begin{aligned} G_{\rm fast} &\equiv G, \quad P_{\rm fast} \equiv A_{\rm CS} PS \\ G_{\rm slow} &\equiv Gg, \quad P_{\rm slow} \equiv A_{\rm ACA} PS. \end{aligned} \tag{4.1}$$

$P_{\rm fast}$ and $P_{\rm slow}$ correspond exactly to the frequency response measurements made in

	Poles	Zeros	Gain
G	150,140,140k	1k,2.3k	83
g	15	none	10

Table 4.1: Required poles, zeros, and gain for the common and auxiliary servo amplifiers. The poles and zeros are given in Hz, and the gain is given in dB.

Figure 3-1. The total loop gain, H, is then

$$H = G_{\rm fast}P_{\rm fast} + G_{\rm slow}P_{\rm slow} \equiv H_{\rm fast} + H_{\rm slow}. \tag{4.2}$$

The point where the gains of the two paths are equal and where control of the servo is passed from one path to the other is known as the *cross-over* point and deserves special attention. The main requirement of the cross-over is that the two paths have a phase difference of less than 180 degrees. If the phase difference between the two paths is 180 degrees, the two paths will fight against each other, adversely effecting the total loop gain at the cross-over point and possibly causing servo instabilities. As long as we can keep the phase difference small, the cross-over should be smooth.

Since we know the response of the plant, which in this case is P_{fast} and P_{slow}, as well as the target design for the full open-loop gain for each path, including the requirements for crossing-over from one path to the other, we can then calculate the requirements for the servo gains $G_{\rm fast}$ and $G_{\rm slow}$. Figure 4-4 shows Bode plots of the requirements, H_α, G_α, and plants, P_α, for both the fast and slow paths. $H_{\rm fast}$ and $H_{\rm slow}$ can also be seen in Figure 4-2 with the total open-loop gain H.

Once we have $G_{\rm fast}$ and $G_{\rm slow}$, it is a simple matter to calculate what we will call the common gain, G, and the auxiliary gain, g. The common and auxiliary gains are what is actually implemented in the servo amplifier control electronics. The calculated pole and zero frequencies, and the required gain for each amplifier are listed in Table 4.1.

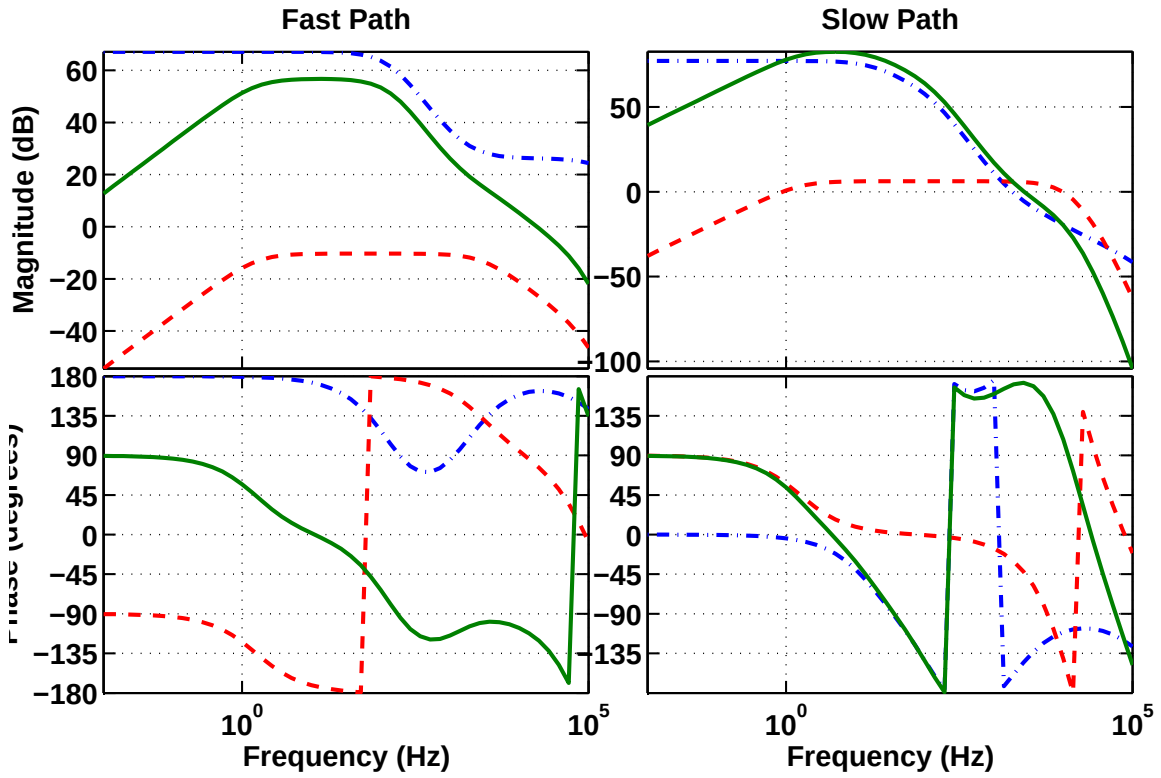

Figure 4-4: Model of the servo frequency response requirements for the fast path (left) and slow path (right). The red curve (dashed) is the plant response, P_α, the green curve (solid) is the total loop gain requirement for the given path, H_α, and the blue curve (dash-dot) is the servo gain requirement for the given path, G_α.

4.4 Servo implementation

The fast and slow paths of the servo were implemented on a single circuit board known simply as the ISS Board. A full circuit schematic can be seen in Appendix E.

The board consists of a series of amplification and filtration stages, each made of simple op-amp circuits. Analog Devices low-noise OP27 op-amps were used for all stages except for the output line drivers, which instead used the Analog Devices AD847 which are capable of driving more current and therefore lower impedance loads.

Initially there was trouble with the electronic ground that created a DC path for the servo signal and caused a DC instability in the servo. The high current being drawn by the photo-diodes caused the ground of the photo-detector to be lifted relative to the ground of the servo board. This ground differential was directly proportional to the current and was therefore effectively a DC signal that was able to bypass the AC coupling filter. Without a non-zero DC reference, any gain at DC will cause the feedback loop to attempt to drive the laser power to zero. This problem was addressed by receiving the signal from the photo-diode differentially. External differential-to-single-ended amplifiers were used to read the photo-detector output at the electronics rack and turn that into a single-ended output that was fed to the servo board input.

Just as with the photo-detector described in Chapter 2, extensive filtering was used to attenuate all signals outside of the servo bandwidth.

This servo provides a gain of greater than 80 dB at 10 Hz, with a bandwidth greater than 30 kHz. Figure 4-5 shows a the open-loop frequency response of the servo, inferred from measurements made of the closed-loop gain.

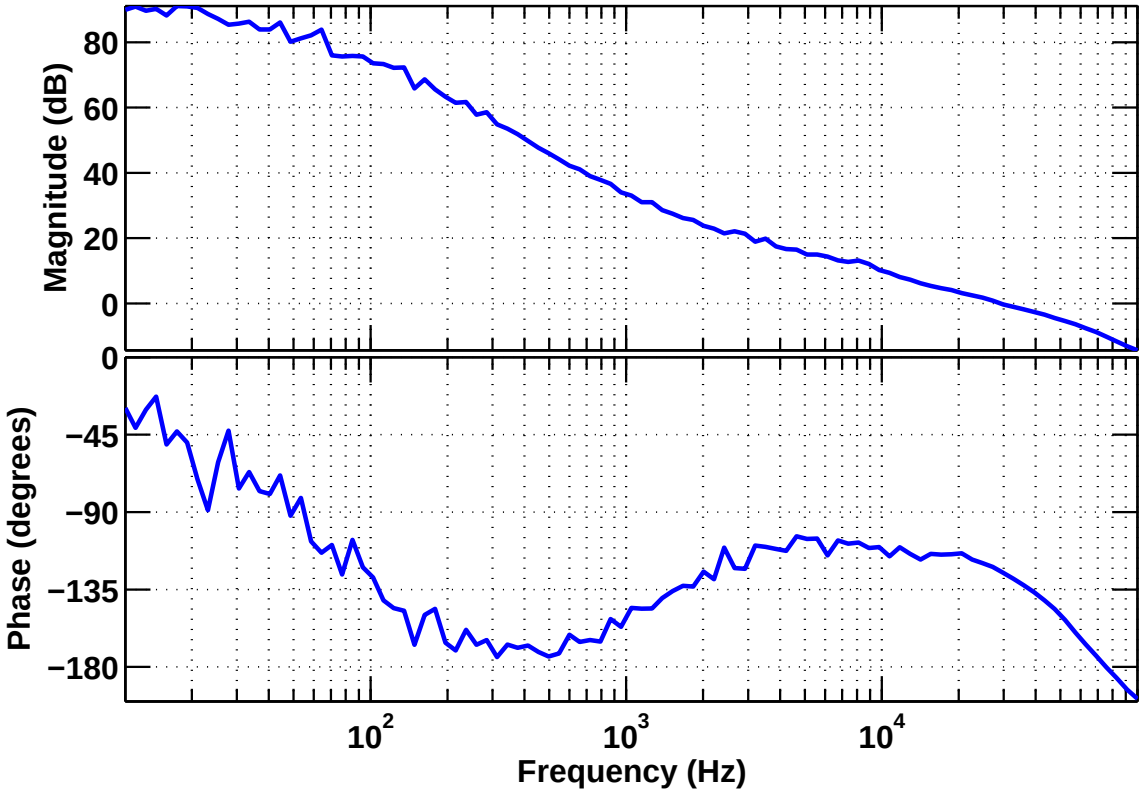

Figure 4-5: Open-loop frequency response of the intensity stabilization servo, derived from a measurement with the loop closed.

Chapter 5

Results and Conclusion

5.1 Results

The present best relative intensity noise level achieved by the servo is about $1\times10^{-8}/\sqrt{\text{Hz}}$ at 10 Hz and about $5\times10^{-9}/\sqrt{\text{Hz}}$ at 100 Hz (Figure 5-1). This level is measured with the *out-of-loop* detector (see Figure 4-1).

The data in Figure 5-1 was taken with a DC photo-current of 140 mA on the out-of-loop photo-detector. This corresponds to an incident light power of 175 mW. However, this relative intensity noise level can be achieved with powers as low as 100 mW.

The achieved intensity noise level is higher than the calculated shot noise level, which at 140 mA is $2\times10^{-9}/\sqrt{\text{Hz}}$ (see Figure 5-1). It is not known at this time what is the limiting factor in these measurements.

Figure 5-1 shows that the noise floor measured by the in-loop photo-diode is well below that measured by the out-of-loop diode, indicating that the achieved intensity noise is not limited by a lack of loop gain in the servo loop between 10 Hz and 150 Hz.

Various electronic noise sources were also carefully characterized. Figure 5-1 also shows the measured input-referred photo-detector dark noise for both the in-loop and out-of-loop detectors, as well as the calculated shot noise level on each detector. The total noise in the measurement is then the quadrature sum of all of these noise sources. This total noise level (shown in pink in Figure 5-1), is about a factor of 3

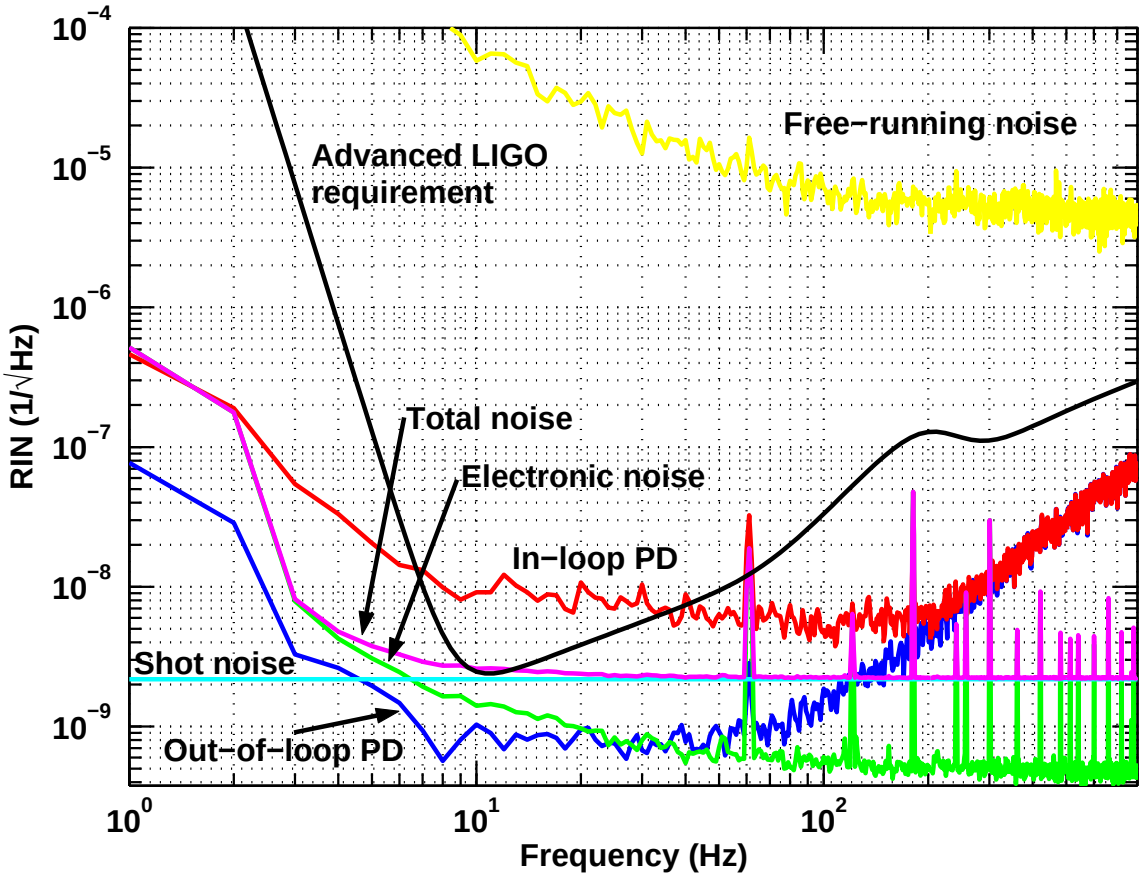

Figure 5-1: Relative intensity noise as measured by in-loop and out-of-loop photodetectors. The expected shot noise and measured electronic noise levels are shown in the light blue and green traces respectively. The black curve shows the Advanced LIGO requirement. (Data taken June 29, 2003.)

less than the measured intensity noise at 10 Hz.

Many potential noise sources where investigated in an attempt to learn what was limiting the achievable intensity noise level.

5.1.1 Detector noise

As mentioned in Section C.6, the first place to look for limits in the servo is in the front end, i.e., the detector. Although the dark noise of the detectors was measured and found to be less that the achievable intensity noise level, it is still possible that there could be noise in the detector that increases as a function of the photo-current.

The bias feedback loop was also investigated as a possible source of power-dependent noise. The photo-detectors were modified so that the photo-diode bias was held constant and was not controlled via feedback. This had no affect on the achievable noise level.

Electronic grounding noise was discovered to be a critical issue. This was not due to EM pick-up, but instead to problems with noise on the ground reference that was adding noise to the signal in the detector. Improvements were made over initial measurements by reading the signals from the photo-detector differentially.

5.1.2 Out-of-band noise

Another challenge is reducing the effect that noise outside the servo bandwidth has on noise in band. The most common cause of this down-conversion of high-frequency noise to lower frequencies is slew rate limits in the electronics.

All amplifiers have a limit to how fast the output can change in response to its input. This slew rate limit is a maximum slope of voltage change and is usually given in units of volts/second. Signals that require voltage changes faster than that allowed by the amplifier slew rate will be distorted, producing a non-linear response in the amplifier. These non-linearities can cause broadband noise, including noise at frequencies significantly below those of the slew rate limited signals.

Since noise due to slew rate limits is only present where there are very fast signals, this noise would not show up in dark noise measurements of the detector, or in open-loop measurements of the electronics noise of the servo amplifier electronics.

Out-of-loop intensity noise measurements showed intensity noise peaks at frequencies of 100 kHz and above. This was discovered very early on in the design of the servo. Consequently, extensive low-pass filtering was used throughout the entire feedback chain to attenuate significantly these out-of-band signals.

5.1.3 Other light noise

The light leaving the PMC is highly polarized, but further polarization filters were used to assure that polarization jitter at the beam splitter would not cause differential intensity variations at the in-loop and out-of-loop photo-diodes.

To eliminate the possibility that frequency noise would be converted to intensity noise in the PMC, a frequency stabilization servo was used to reduce the frequency noise of the laser [1] with no improvements in the intensity noise.

5.1.4 External noise

Finally, extensive measures were also taken to reduce the effects of any possible environmental noise sources. For instance, neutral density filters were placed in front of the photo-detectors in order to minimize the effects of scattered light, and the entire experiment was placed in an enclosure that significantly reduced the amount of acoustic noise and the effects of air currents, once again with minimal effect.

In fact, at one point the beam jitter on the detector was made worse by vibrating one of the steering mirrors. The jitter was measured by a quad photo-detector and was made a made worse by a factor of two. No increase was observed in the achievable noise level. This was taken as an indication that the experiment was probably not limited by beam jitter on the face of the detector.

5.2 Conclusion

Further work is required to achieve the extremely demanding intensity stabilization requirement of Advanced LIGO. Planned improvements include the development of in-vacuum photo-detectors to further remove external noise sources, moving the detectors after the LIGO suspended modecleaner in an attempt to reduce beam jitter further, and the use of multiple in-loop detectors to increase the total measured signal-to-noise ratio.

Other researchers have observed a similar performance at 100 Hz utilizing a dif-

ferent photo-detector design [23]. At present it is not know what is limiting the noise performance of either experiment at this level.

In conclusion, we have achieved intensity stabilization of a solid state laser at the $1\times10^{-8}/\sqrt{\text{Hz}}$ level at 10 Hz. To our knowledge this is the first time that such performance has been reported.

Appendix A

Shot Noise

Shot noise, or photon counting noise, is a fundamental noise source due to the quantum nature of light. Light is made up of photons. The photons from a beam of light do not arrive at the detector at a constant rate. Instead, there is a fluctuation in the rate of arrival that is determined by *Poisson statistics* [19, 20, 25] and is characterized by a probability distribution $p(N)$ known as the *Poisson distribution*[1]:

$$p(N) = \frac{\langle N \rangle^N e^{-\langle N \rangle}}{N!}, \tag{A.1}$$

where N is the number of events (in this case photon arrivals) per counting interval, τ, and $\langle N \rangle$ is the mean number of events. An important and relevant property of this distribution is that when $\langle N \rangle \gg 1$, the Poisson distribution can be approximated by a *Gaussian distribution* with a standard deviation given by $\sigma_{\langle N \rangle} = \sqrt{\langle N \rangle}$.

If one were to then try to determine the arrival rate of photons per second, $\langle n \rangle = \langle N \rangle / \tau$, by making measurements lasting τ seconds, they would find that the fractional

[1]The fact that the quantum state of a gain-saturated laser has a Poisson distribution of photon emission is not trivial to derive and is a bit outside of the scope of this thesis [20, 25]. It should also be noted that it is possible to tailor the states of the radiation field such that the amplitude fluctuations can be reduced below the shot noise level at the expense of an increase in phase fluctuations. This is a process known as *squeezing*.

fluctuations of each measurement would be given by

$$\frac{\sigma_{\langle N\rangle}}{\langle N\rangle} = \frac{\sqrt{\langle n\rangle\tau}}{\langle n\rangle\tau} = \frac{1}{\sqrt{\langle n\rangle\tau}}. \tag{A.2}$$

The important thing to note about this formula is that as $\langle n\rangle\tau$ increases, the fractional fluctuations decrease, and the precision of the measurement increases.

Each photon carries an energy of $h\nu = h/c\lambda$, with h being Planck's constant, ν the frequency of the photon, λ the wavelength, and c the speed of light. The mean power, $\langle P\rangle$, in a given beam of light is then equal to the arrival rate of photons per second, $\langle n\rangle$, times the energy per photon:

$$\langle P\rangle = \langle n\rangle h\nu = \frac{\langle n\rangle hc}{\lambda}. \tag{A.3}$$

If this equation is then plugged into equation A.2, we see that the fractional fluctuations in the photon arrival is given by:

$$\frac{\sigma_{\langle N\rangle}}{\langle N\rangle} = \sqrt{\frac{hc}{\lambda\langle P\rangle\tau}} \tag{A.4}$$

Since the arrival of the photons is random, there is no preferred time scale. This means that the amplitude spectral density of equation A.4 is flat and the photon shot noise at the detector can then be expressed as:

$$e_{\text{shotnoise}}(f) = \sqrt{\frac{hc}{\lambda\langle P\rangle}}. \tag{A.5}$$

where in this case $\langle P\rangle$ is the mean of the power over the length of the measurement (or one over the measurement bandwidth) [2]. Equation A.5 is therefore a relative intensity noise *amplitude spectral density* and has units of $1/\sqrt{\text{Hz}}$.

[2] An important thing to note here is that the shot noise level from Equation A.5 is inversely proportional to square root of the light power, P. In other words, increasing the power decreases the noise associated with fluctuations in the arrival rate of the photons at the detector. This is of great significance to LIGO and is driving the development of high-power lasers for use in advanced LIGO, as noted in Chapter 1. This can only take you so far, though, since higher light powers also mean higher *radiation pressure noise*.

Appendix B

Amplifier Noise

Modern low noise signal pre-amplifiers are usually made with integrated circuit operation amplifiers, or *op-amps*. Op-amps are simple differential amplifiers with two high-impedance inputs and a single low-impedance output [13]. The output is the difference of the voltages at the noninverting and inverting inputs, multiplied by a very high gain factor. Op-amps are often run in current feedback configurations, enabling precise control of the gain of the system. See Chapters 4 of reference [13] for an in-depth description of op-amps and op-amp circuits.

The total noise of an amplifier with a signal source resistance, R_S (Figure B-1), is:

$$e_A = \sqrt{e_a^2 + (i_a R_S)^2} \tag{B.1}$$

where e_a and i_a are the amplifiers voltage and current noise. For op-amp amplifiers, e_a and i_a are further functions of the inherent voltage and current noise of the op-amp integrated circuit, e_n and i_n, as well as the feedback resistors used to set the amplifier's gain.

For **Noninverting** amplifiers, Figure B-2a:

$$i_a^2 = i_n^2 \tag{B.2}$$

$$e_a^2 = e_n^2 + 4kTR_{\|} + (i_n R_{\|})^2 \tag{B.3}$$

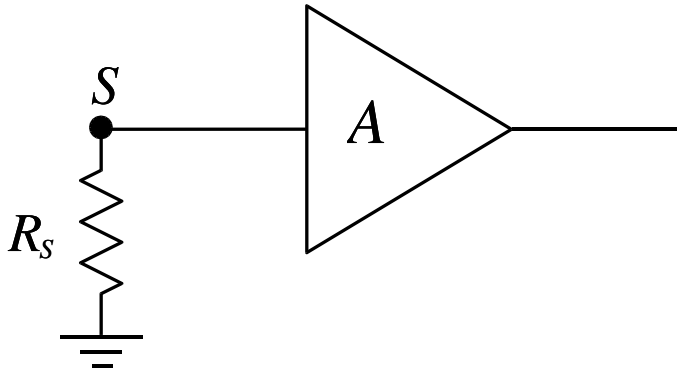

Figure B-1: Amplifier model.

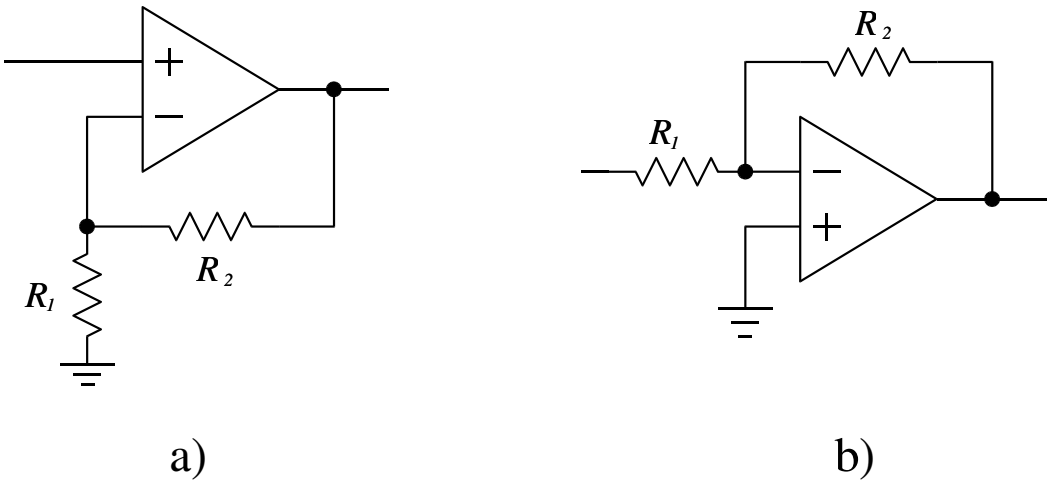

Figure B-2: Amplifier configurations. a) noninverting, b) inverting.

where

$$R_{\|} = \frac{R_1 R_2}{R_1 + R_2}. \tag{B.4}$$

and the factor $4kTR_{\|}$ is the *Johnson noise* of the feedback resistors, with k as Boltzmann's constant and T is the absolute temperature in Kelvin.

For **Inverting** amplifiers, Figure B-2b:

$$i_a^2 = i_n^2 + 4kT\frac{1}{R_2} \tag{B.5}$$

$$e_a^2 = e_n^2 + (i_a R_1)^2 \tag{B.6}$$

Equations B.3 and B.6 are combined with Equation B.1 to determine the overall noise of an amplifier, e_A. The total noise at the point S in Figure B-1 is now the quadrature sum of the noise from the amplifier and the Johnson noise of the source impedance:

$$e_S = \sqrt{e_A^2 + 4kTR_S} \tag{B.7}$$

The signal-to-noise ratio (SNR) of the system is the signal voltage at S divided by the voltage noise at S:

$$SNR = \frac{v_S}{e_S} \tag{B.8}$$

See Chapter 7 of reference [13] for a further discussion of amplifier noise.

Appendix C

Introduction to Feedback Control Systems

One of the most important technical theories behind LIGO is the concept of feedback control. Feedback control systems are involved in almost every aspect of the experiment from top to bottom. The entire interferometer is controlled by feedback control systems, as well as nearly every single individual subsystem. Because of this, it is critical to understand at least the basics of feedback control theory and what they can do.

This appendix will be a very simple and basic introduction to linear, time-invariant control systems. Control system theory is an entire field of engineering unto itself, and therefore countless texts have been written on the subject. For a more complete introduction to the field, please refer to these books: [4, 15, 8].

C.1 Block diagrams

There are four primary elements of a feedback control system: the *plant, sensor, amplifier*, and *actuator*. The plant is the system that we wish to control. The sensor is the component that monitors the plant and produces the error signal when the plant deviates from a given reference value. The amplifier is used to filter and amplify the error signal in order to shape the feedback loop's transfer function. This is necessary

to ensure that the the loop is stable (see Section C.4. Finally, the actuator is the element that receives the filtered and amplified error signal and supplies the feedback to the plant.

The easiest way to understand control systems is to study the illustrative concept of *block diagrams*. In block diagrams, each element of the servo systems is represented by a block in the diagram. The symbols used to designate each block represent the mathematical operation that the block performs on its input. Since we are only dealing with linear, time-invariant systems here, this mathematical function is linear and the output of each element is a linear function of the input. These functions are referred to as the *transfer function*.

Figure C-1 is an example of a block diagram for a simple feedback control system. The symbol $\bigoplus$ denotes a *summing point* where the output is the algebraic sum of the inputs, and $\bullet$ is a *takeoff point* where each output is equal to the input.

C.2 Feedback

To understand the true beauty of feedback control, we must investigate how a system behaves once the loop has been closed. In Figure C-1, the plant, sensor, amplifier and actuator transfer functions are denoted by the blocks P, S, G, and A, respectively. (All signals, X_α, and systems, H, are understood to be functions of frequency, f, or the Laplace variable, s, (see Section C.3) although the dependence will not be explicitly stated.)

We begin by defining a new parameter known as the total *open-loop gain* of the system, $H \equiv PSGA$. This is the transfer function of all servo elements in series. Now let us look at the system transfer function between the input X_d and the point in servo immediately after it, X_i, with all other inputs held at zero:

$$X_i = X_d - X_o = X_d - H \cdot X_i$$

$$X_i = \tfrac{1}{1+H} X_d. \tag{C.1}$$

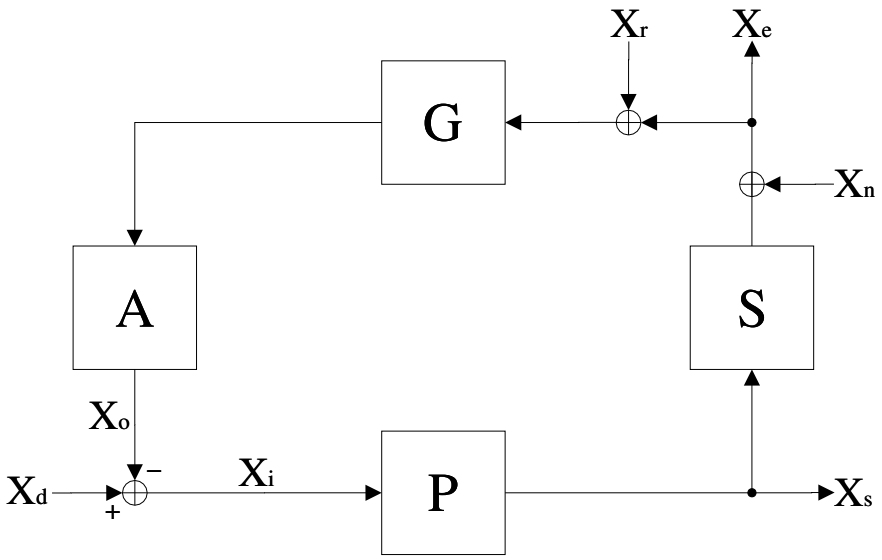

Figure C-1: Simple feedback control block diagram.

The factor $1/(1+H)$ is known as the *closed-loop gain* of the system, and it illustrates the full power of the feedback control system. If $H \gg 1$, the closed-loop gain goes to zero. The signal acting on the plant, X_i, then goes to zero as well. If X_d is some sort of external disturbance that is causing noise, the feedback loops acts to suppress this disturbance. However, the component transfer functions, and therefore the open- and closed-loop gains of the systems, are complex functions and will vary over different frequencies, as described in the next section. The goal then is to make H as large as possible at the frequencies where you wish to make the disturbance go to zero.

C.3 Transfer functions

For linear, time-invariant control system analysis, it is most common to work in the frequency domain. We therefore look at the *Laplace transform* of the time-domain signals:

$$\mathcal{L}[f(t)] \equiv F(s) \equiv \int_0^\infty f(t)e^{-st}\,dt \tag{C.2}$$

The Laplace transform takes a function of time, $f(t)$, and produces a function of a complex frequency, $F(s)$, where $s = \sigma + i\omega$.

The transfer function of a component is simply (ignoring initial values) the ratio of the Laplace transform of the output signal of the component, $Y(s)$, to the Laplace transform of the input signal, $U(s)$. The transfer function then takes the form,

$$X(s) = \frac{Y(s)}{U(s)}. \tag{C.3}$$

Laplace transforms are usually written as polynomials of s. Transfer functions are then ratios of polynomials of s. The polynomials are usually written factored, so transfer functions usually have the form:

$$X(s) = \frac{k \prod_{i=1}^{m}(s + z_i)}{\prod_{i=0}^{n}(s + p_i)}. \tag{C.4}$$

The roots of these polynomials have particular significance. The roots of the numerator, z_i, are called system *zeros*, since that is where the transfer function goes to zero, and the roots of the denominator, p_i are the system *poles*, where the function is infinite. The factor k is the overall gain of the transfer function.

C.4 Stability

For a feedback control system to be useful, it must be stable. This is an absolute requirement. Stability means that the the output is bounded if the input is bounded. If the output is not bounded, the system is unstable and certain bounded inputs could cause the system to oscillate out of control.

Probably the most important parameter of the system in determining the system stability is the total open-loop gain, H. It is from this parameter that we gain the most insight into the behavior of the system. Lets start by looking back at the expression for the closed-loop gain in Equation C.1. What happens when $H = -1$? Obviously, the closed-loop gain of the system blows up and the output will go to infinity no matter what the input disturbance.

When determining stability, it is important to note what happens to the open-loop transfer function as the gain approaches unity and the phase approaches $-180°$. What we look for, then, are the gain and phase margins of the transfer function. The *gain margin* is defined as the amount that the gain is below unity at the point that the phase crosses $-180°$. The *phase margin* is defined as the phase greater than $-180°$ at the point that the gain crosses unity. The system is said to be stable if gain margin is greater than 6 dB and phase margin is greater than 30°. Systems are usually stable if these margins are greater than 0. The larger they are, the more stable the system.

As one might imagine, the gain and phase margins are heavily dependent on the poles and zeros of the system, as discussed in the next section.

C.5 Bode analysis

A very convenient way to analyze a feedback control system is to use what is known as *Bode analysis*. In this technique, the Laplace variable, s, in the transfer function is replaced with $i\omega$ to produce a complex function of frequency, ω. We then separately plot both the magnitude and phase of the transfer function of the system as a function of frequency.

Figure C-2 is an example of a Bode plot of a transfer function. In this figure, we also illustrate the effects of a simple pole or a simple zero on the frequency response. If we look at the asymptotic behavior of a poles (blue in Figure C-2), we see that the magnitude and phase are flat at low frequencies, then, at the frequency of the pole (which in this case is 10 Hz), the magnitude begins to fall at a rate of -20 dB/decade, while the phase drops by 90°. Zeros produce just the opposite effect, with the magnitude turning to rise at a rate of 20 dB/decade, while the phase rises by 90°.

Bode plots allow one to easily identify the phase and gain margins and therefore examine the relative stability of the system. We can also easily see what effects poles and zeros have on stability. Two uncompensated poles, for instance, will cause the gain to asymptotically approach -40 dB/decade at high frequencies. More im-

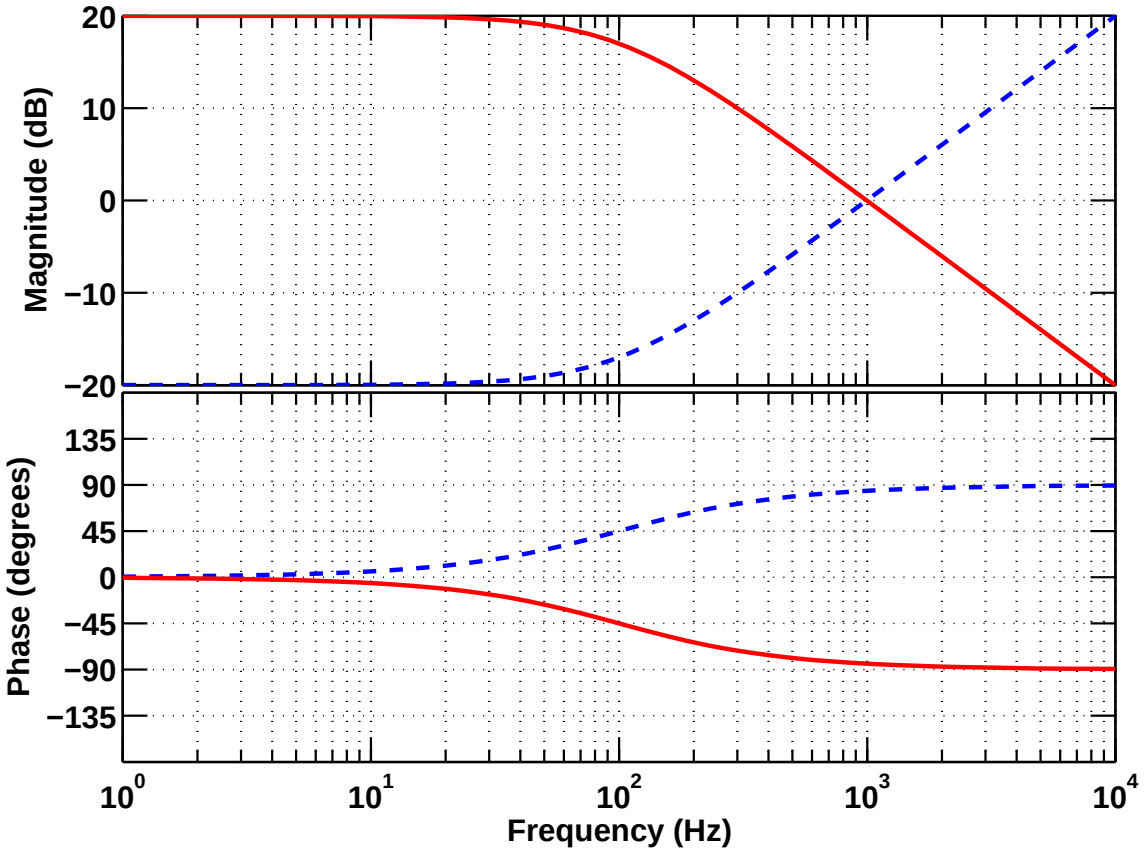

Figure C-2: Bode plot of a simple pole with an overall gain of 20 dB (red solid) and a simple zero with an overall gain of -20 dB (blue dashed).

portantly, it will cause the phase to drop by 180°. This means that the unity gain crossing would have to be before the second pole to assure sufficient phase margin.

C.6 Limitations and noise

There are two things that can limit the effectiveness of a servo, lack of gain and noise. If we look back to Equation C.1, we see that the amount of suppression of the disturbance provided by the servo is limited to how small the closed-loop gain is. The closed-loop is limited by how large the open-loop is. The goal is to get the open-loop gain as large as possible. However, there are practical limits to how large the open-loop gain can be. Servo that do not have enough gain are referred to as *gain limited*.

To see where the noise limitations of the system are, let us return to the analysis of Figure C-1. The error signal for the servo, X_e, comes from the sensor, S. However, like every system in the real world, the sensor is not immune from noise. The sensor noise, labeled, X_n in the figure, affects the error signal.

Appendix D

Photo-detector Circuit Diagram

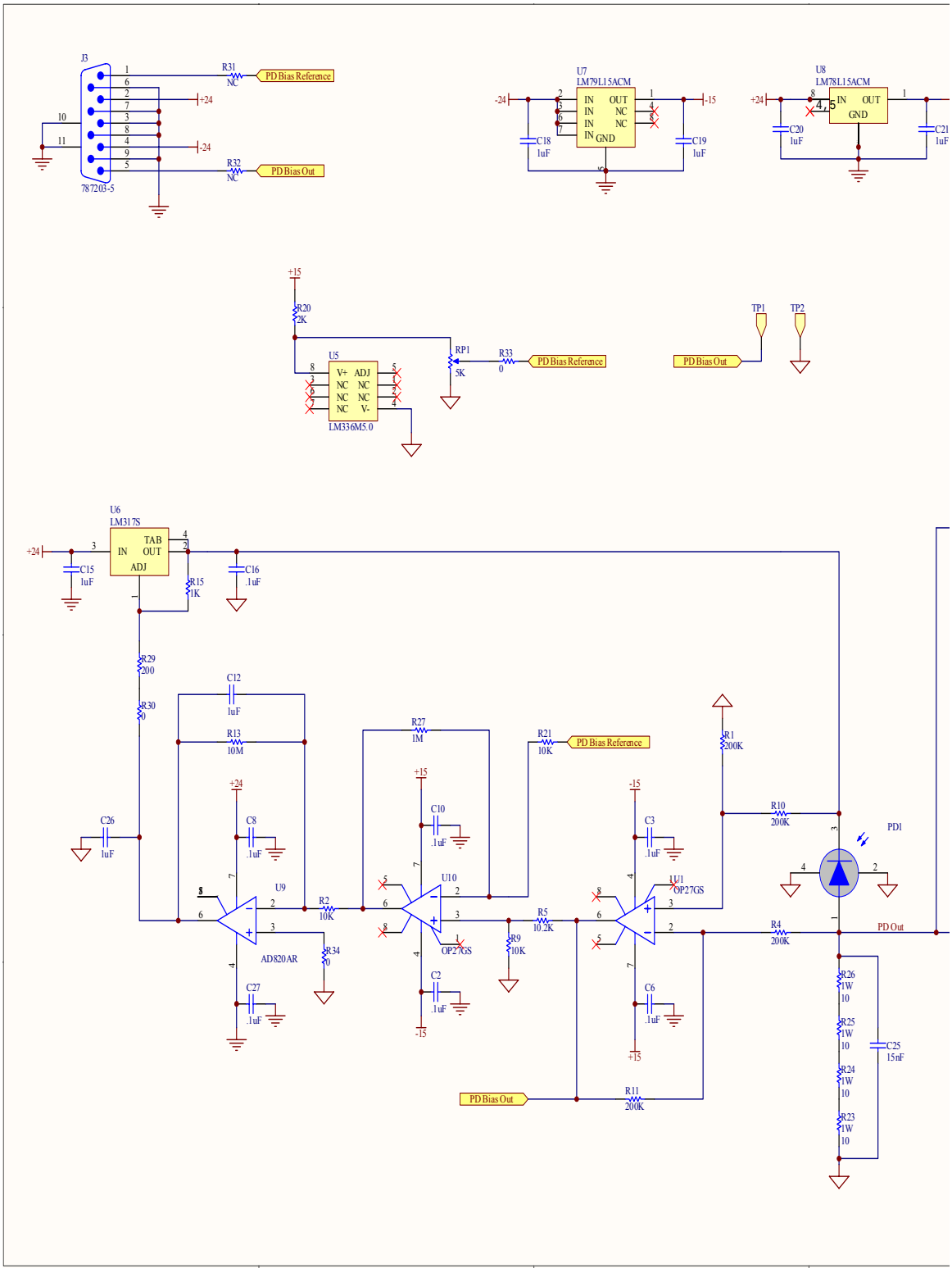

Figure D-1: Full circuit diagram of the photo-detector. (Continued on next page.)

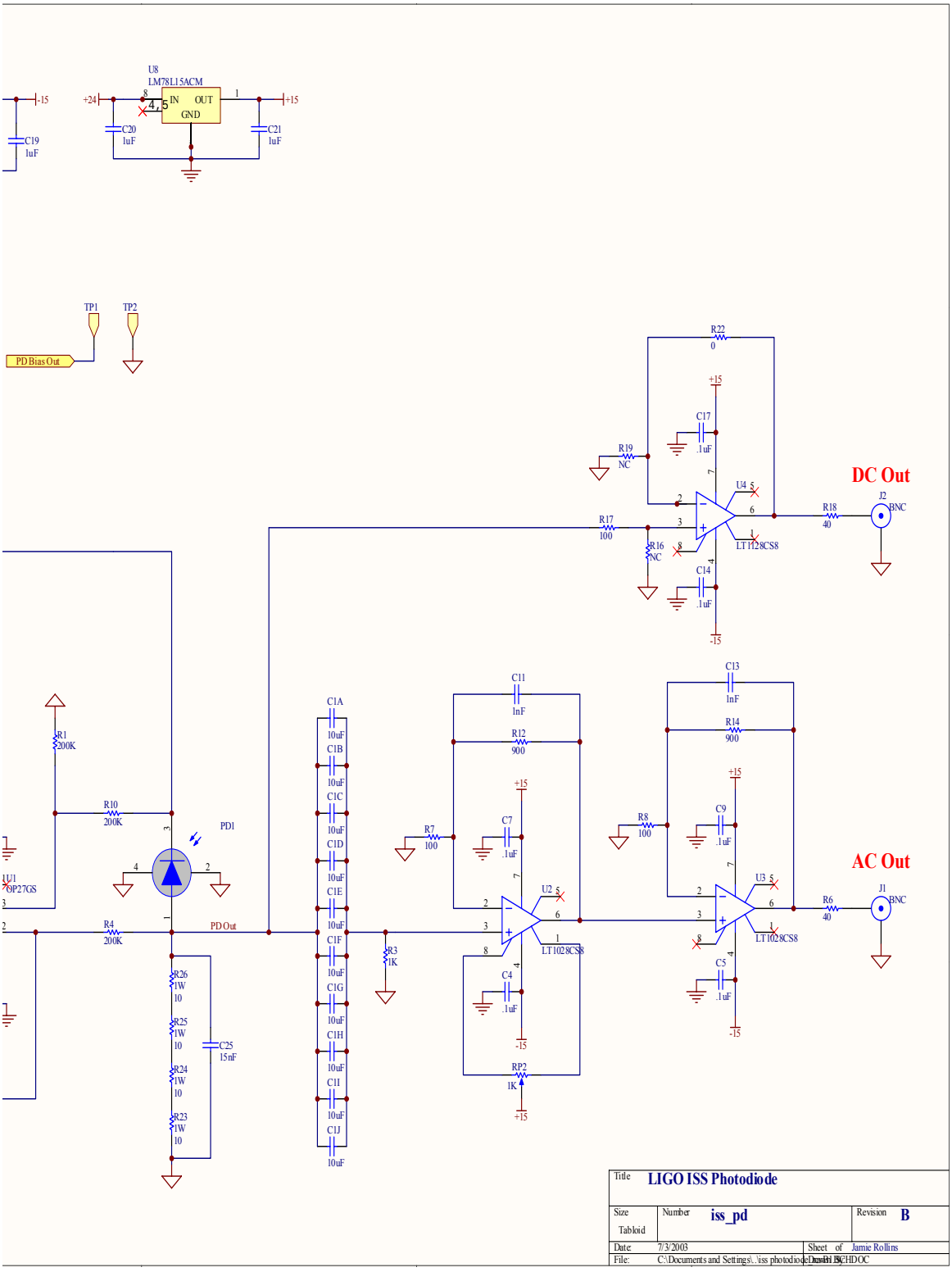

Figure D-2: Full circuit diagram of the photo-detector.

Appendix E

Servo Board Circuit Diagram

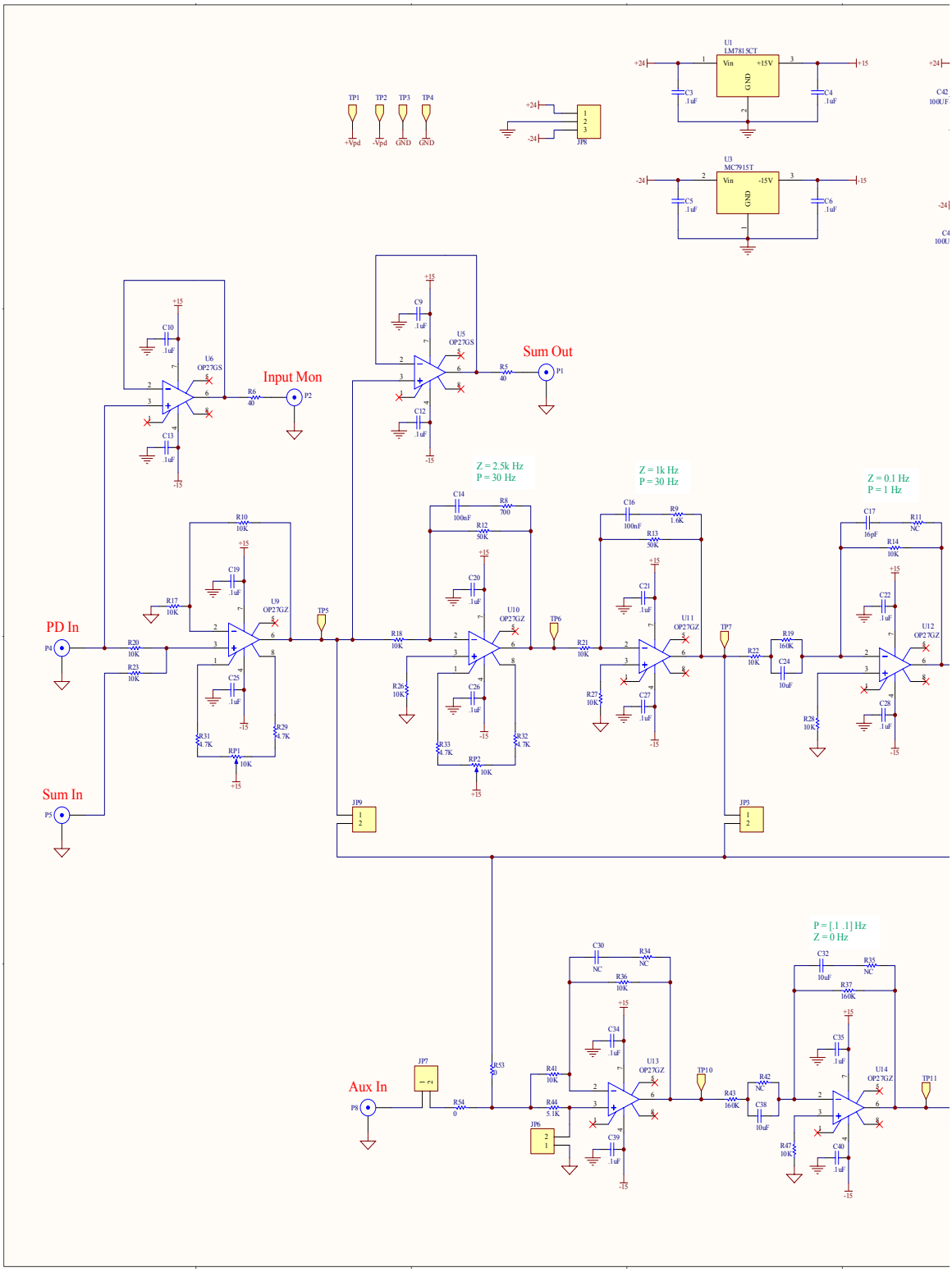

Figure E-1: Full circuit diagram of the intensity stabilization servo board. (Continued on next page.)

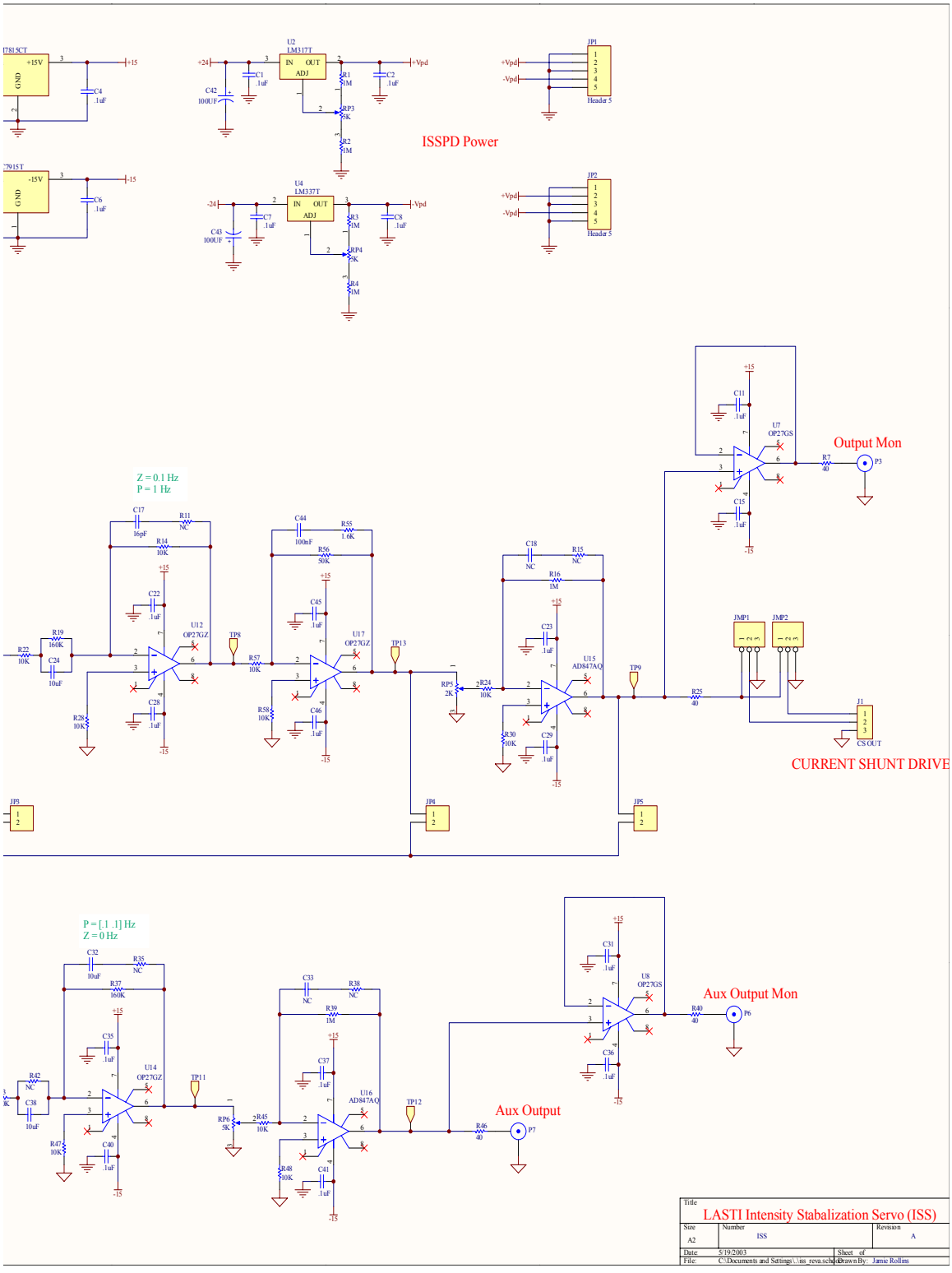

Figure E-2: Full circuit diagram of the intensity stabilization servo board.

Bibliography

[1] R. Abbott and P. King. Control system design for the ligo pre-stabilized laser. Technical report, LIGO Scientific Collaboration, November 2001. LIGO-P010037-00-c.

[2] R.S. Abbott and P.J. King. Diode-pumped Nd:YAG laser intensity noise suppression using a current shunt. *Review of Scientific Instruments*, 72:1346, February 2001.

[3] A. Abramovici, W. Althouse, R. Drever, Y. Gürsel, S. Kawamura, F. Raab, D. Shoemaker, L. Sievers, R. Spiro, K. Thorne, R. Vogt, R. Weiss, S. Whitcomb, and M. Zucker. Ligo-the laser interferometer gravitational-wave observatory. *Science*, 256:325–333, 1992. LIGO-G920010-00-R.

[4] Alex Abramovici and Jake Chapsky. *Feedback Control Systems: A Fast-Track Guide for Scientists and Engineers.* Kluwer Academic Publishers, 2000.

[5] B. Barish and R. Weiss. LIGO and the detection of gravitational waves. *Phys. Today*, 52:44, October 1999.

[6] R.W.P. Drever, N. Uehara, F.V. Kowalski, J. Hough, and G.M. Ford. Laser phase and frequency stabilization using an optical resonator. *Appl. Phys.*, 31:97, 1983.

[7] Alejandro D. Farinas, Eric K. Gustafson, and Robert L. Byer. Frequency and intensity noise in an injection-locked, solid-state laser. *J. Opt. Soc. Am. B*, 12:328, 1995.

[8] Gene F. Franklin, J. David Powell, and Abbas Emami-Naeini. *Feedback Control of Dynamic Systems*. Addison-Wesley, third edition, 1994.

[9] Peter Fritschel. Advanced ligo systems requirements review. Technical report, LIGO Scientific Collaboration, July 2001. LIGO-G010242-00-D.

[10] Malcolm Gray. Australian National University, Department of Physics and Theoretical Physics, Faculty of Science, Australian National University, ACT 0200, Australia, (personal communication 2003).

[11] E. Gustafson, D. Shoemaker, K. Strain, and R. Weiss. LSC white paper on detector research and development. Technical report, LIGO Scientific Collaboration, September 1999. LIGO-T990080-00-D.

[12] Charles C. Harb, Timothy C. Ralph, Elanor H. Huntington, Ingo Freitag, David E. McClelland, and Hans-A. Bachor. Intensity-noise properties of injection-locked lasers. *Physical Review A*, 54(5), 1996.

[13] Paul Horowitz and Winfield Hill. *The Art of Electronics*. Cambridge University Press, second edition, 1989.

[14] Lightwave Electonics Inc. MOPA Series 6000 Laser, SN #110.

[15] III Joseph J. DiStefano, Allen R. Stubberud, and Ivan J. Williams. *Feedback and Control Systems*. Schaum's Outline Series, McGraw-Hill, second edition, 1995.

[16] John H. Moore, Christopher C. Davis, and Michael A. Coplan. *Building Scientific Apparatus*. Perseus Books, second edition, 1991.

[17] D.J. Ottaway, P.J. Veitch, C. Hollitt, D. Mudge, and M.W. Hamilton. Frequency and intensity noise of an injection-locked Nd:YAG ring laser. *Appl. Phys. B*, 71:163, 2000.

[18] Bahaa E. A. Saleh and Malvin Carl Teich. *Fundamentals of Photonics*. John Wiley & Sons, 1991.

[19] Peter R. Saulson. *Fundamentals of Interferometric Gravitational Wave Detectors*. World Scientific, 1994.

[20] Marlan O. Scully and M. Suhail Zubairy. *Quantum Optics*. Cambridge University Press, 1997.

[21] Anthony E. Siegman. *Lasers*. University Science Books, 1986.

[22] B. Willke, N. Uehara, E.K. Gustafson, R.L. Byer, and P.J. King. Spatial and temporal filtering of a 10-W Nd:YAG laser with a fabry-perot ring-cavity premodecleaner. *Optics Letters*, 23:1704, November 1998.

[23] Benno Willke. Institute for Atomic and Molecular Physics, University of Hannover, Callinstr. 38, D-30167 Hannover, Germany, (personal communication 2003).

[24] Benno Willke. Update on advanced ligo psl program. In *LIGO LSC Meeting*, Hanford, WA, August 2002. LIGO Scientific Collaboration. LIGO-G020334-00-Z.

[25] Amnon Yariv. *Quantum Electronics*. John Wiley & Sons, third edition, 1989.